ICES REPORT 17-21

September 2017

Error Estimates for Dynamic Augmented Lagrangian Boundary Condition Enforcement, with Application to Immersogeometric Fluid–Structure Interaction

by

Yue Yu, David Kamensky, Ming-Chen Hsu, Xin Yang Lu, Yuri Bazilevs, and Thomas J.R. Hughes

The Institute for Computational Engineering and Sciences
The University of Texas at Austin
Austin, Texas 78712

Reference: Yue Yu, David Kamensky, Ming-Chen Hsu, Xin Yang Lu, Yuri Bazilevs, and Thomas J.R. Hughes, "Error Estimates for Dynamic Augmented Lagrangian Boundary Condition Enforcement, with Application to Immersogeometric Fluid–Structure Interaction," ICES REPORT 17-21, The Institute for Computational Engineering and Sciences, The University of Texas at Austin, September 2017.

Mathematical Models and Methods in Applied Sciences

ERROR ESTIMATES FOR PROJECTION-BASED DYNAMIC AUGMENTED LAGRANGIAN BOUNDARY CONDITION ENFORCEMENT, WITH APPLICATION TO FLUID–STRUCTURE INTERACTION

YUE YU*

Department of Mathematics, Lehigh University,
14 East Packer Avenue, Bethlehem, PA 18015, USA
yuy214@lehigh.edu

DAVID KAMENSKY

Department of Structural Engineering, University of California, San Diego,
9500 Gilman Drive, Mail Code 0085, La Jolla, CA 92093, USA
dmkamensky@eng.ucsd.edu

MING-CHEN HSU

Department of Mechanical Engineering, Iowa State University,
2025 Black Engineering, Ames, IA 50011, USA
jmchsu@iastate.edu

XIN YANG LU

Department of Mathematical Sciences, Lakehead University,
955 Oliver Road, Thunder Bay, ON P7B 5E1, Canada
Department of Mathematics and Statistics, McGill University,
805 Sherbrooke St W, Montreal, QC H3A 0B9, Canada
xlu8@lakeheadu.ca

YURI BAZILEVS

School of Engineering, Brown University,
184 Hope St., Providence, RI 02912, USA
yuri_bazilevs@brown.edu

THOMAS J. R. HUGHES

Institute for Computational Engineering and Sciences, The University of Texas at Austin,
201 East 24th St, Stop C0200, Austin, TX 78712, USA
hughes@ices.utexas.edu

Received (Day Month Year)
Revised (Day Month Year)
Communicated by (xxxxxxxxxx)

*Corresponding author

In this work, we analyze the convergence of the recent numerical method for enforcing fluid–structure interaction (FSI) kinematic constraints in the immersogeometric framework for cardiovascular FSI. In the immersogeometric framework, the structure is modeled as a thin shell, and its influence on the fluid subproblem is imposed as a forcing term. This force has the interpretation of a Lagrange multiplier field supplemented by penalty forces, in an augmented Lagrangian formulation of the FSI kinematic constraints. Because of the non-matching fluid and structure discretizations used, no discrete *inf-sup* condition can be assumed. To avoid solving (potentially unstable) discrete saddle point problems, the penalty forces are treated implicitly and the multiplier field is updated explicitly. In the present contribution, we introduce the term *dynamic augmented Lagrangian* (DAL) to describe this time integration scheme. Moreover, to improve the stability and conservation of the DAL method, in a recently-proposed extension we projected the multiplier onto a coarser space and introduced the projection-based DAL method. In this paper we formulate this projection-based DAL algorithm for a linearized parabolic model problem in a domain with an immersed Lipschitz surface, analyze the regularity of solutions to this problem, and provide error estimates for the projection-based DAL method in both the $L^\infty(H^1)$ and $L^\infty(L^2)$ norms. Numerical experiments indicate that the derived estimates are sharp and that the results of the model problem analysis can be extrapolated to the setting of nonlinear FSI, for which the numerical method was originally proposed.

Keywords: immersogeometric method; fluid–structure interaction (FSI); augmented Lagrangian method; parabolic initial-boundary value problem; sub-optimal error estimates; Lipschitz domain.

AMS Subject Classification: 65M12, 65M60, 65M15, 74F10

Contents

1. Introduction

Recent years have seen great interest in numerical analysis of fluid–structure interaction (FSI) [1–26] due to its relevance to structural [27, 28], biomedical [29], and other engineering applications [30]. In a recent series of articles [31–36], a framework for simulating FSI dynamics of thin, flexible shell structures immersed in a viscous, incompressible fluid was developed, where it was assumed that the thin structure can cut through the fluid meshes and the fluid/structure meshes do not have to match each other on the fluid–structure interface [37–39]. The target application was bioprosthetic heart valve [40] analysis. Heart valves are anatomical structures in the heart, regulating the direction of blood flow. Bioprosthetic heart valves are artificial replacements for diseased valves that mimic the structure of native valves: they consist of several thin elastic leaflets that are pushed open by flow in one direction and shut by flow in the other direction. FSI analysis could become an important tool for understanding and designing bioprosthetic heart valves; however, this problem class presents special difficulties [41–43]: (1) due to the thinness of the heart valve leaflets, shell models are typically employed for efficiency. However, the high-order derivatives in some shell models (e.g., Kirchhoff–Love shells [44]) require additional smoothness of the numerical solutions; (2) in heart valve problems the fluid and structure densities are close. Convergence of coupled solvers is problematic because of the "added-mass" effect [45]; (3) the fluid velocity gradients and blood pressure are discontinuous across the leaflets, which is difficult to approximate in unfitted discretizations; (4) the leaflets undergo large deformation and contact in each cardiac cycle, which cause significant changes in the geometry and reduce the boundary regularity of the region occupied by fluid.

To accommodate large deformations of and contact between bioprosthetic heart valve leaflets, [31] pursued an immersed boundary numerical method (see, e.g., [16–18, 46]), in which the fluid and structure are discretized separately and coupled in the numerical method. To simplify the translation of bioprosthetic heart valve designs into analysis models, [31] used an isogeometric discretization [47, 48] of the bioprosthetic heart valve leaflets, representing discrete approximations to the valve's deformation with the same spline function space used to design its geometry. Moreover, isogeometric spline spaces can be as smooth as the geometry allows, which permits straightforward discretization of fourth-order thin shell models. The term *immersogeometric analysis* was introduced in [31], to identify the idea of directly using design geometries as immersed boundaries. References [28, 49–51] explore immersogeometric analysis in several application areas, using a variety of numerical methods.

This paper focuses on the recent numerical method introduced in [36], which can be seen as a modification of the original immersogeometric method proposed in [31]. This numerical method is specialized for problems in which the structure is modeled geomet-

rically as a surface of co-dimension one to the fluid subproblem domain. The interaction between the shell structure and fluid is mediated by a Lagrange multiplier field, which enforces the constraint that the fluid and shell structure velocities match along the shell structure's midsurface. Immersed boundary numerical methods based on this distributed Lagrange multiplier concept have their origins in the work of Glowinski and collaborators [52, 53], and continue to be studied today by Boffi, Gastaldi and Cavallini [22, 54]. In [53], a Lagrange-multiplier-based fictitious domain method is presented and tested on a fluid–solid coupling problem, where both the fluid and solid subdomains are in 2D. In this method, the fluid flow equations are enforced in the whole domain, including the solid subdomain, and the solid boundary is constrained using a distributed Lagrange multiplier. In [22], the authors provided optimal error estimates for the Lagrange-multiplier based fictitious domain method on a simplified linear model for the solid. Besides the case when the fluid and solid have the same dimension, the authors have further discussed the case of a thin solid immersed in a fluid. However, in [22] the error estimates depend on the problem regularity, i.e., the smoothness of the solutions, which was not discussed in the paper. Moreover, the Lagrange-multiplier based fictitious domain method entails the construction of a saddle point problem, which is fraught with practical difficulties in the discrete setting.

Drawing inspiration from discrete optimization [55, 56] and solution methods for contact problems [57] (where non-matching discretizations are the norm), [31] attempted to use an augmented Lagrangian iteration. This iteration avoids directly solving a saddle point problem by introducing auxiliary penalty forces, then alternating between 1: solving an unconstrained problem, with fixed Lagrange multipliers, and 2: using the penalty forces to update the Lagrange multipliers. Finding the convergence of this iteration unreliable, [31] truncated the original augmented Lagrangian iteration, updating the Lagrange multiplier only once each time step. This can be reinterpreted as an implicit discretization of the feedback forcing method of Goldstein et al. [58–62], in which the fluid–structure forcing (i.e. Lagrange multiplier) is governed by a stiff differential equation in time, essentially penalizing the time integral of fluid–structure velocity discrepancy [31, Section 4.3]. Feedback forcing is a rate form of the fluid–structure *displacement* penalties [63, Section 4.2.1] used quite widely to simulate airbag inflation [64], heart valve FSI [65–68], and other fluid–thin structure interaction phenomena [69–71]. Retaining the Lagrange multiplier viewpoint leads to stabilization schemes [34, 36] that would not clearly emerge from the picture of accumulating a fluid–structure displacement difference in rate form and penalizing it. In this paper, we introduce the term *dynamic augmented Lagrangian* (DAL) to describe the resulting family of numerical methods for imposing the Dirichlet boundary conditions on the fluid–structure interface. The idea of DAL was initially introduced for immersogeometric analysis in [31], and came from a combination of heuristic analogies to feedback methods and results of numerical experiments. However, wildly oscillatory multiplier fields were observed in the original DAL method. The authors then proposed the projection-based DAL method [36] by projecting the Lagrange multiplier into a coarse mesh, and showed numerically that this projection-based method efficiently controls the numerical oscillations of the Lagrange multiplier and enhances the kinematic constraint on the interface velocities in the steady limit. That means, when applying the projection-based

DAL method to a steady problem, with the mesh size $h \to 0$ the integral of numerical solution is equal to the integral of the given Dirichlet condition on the interface, which is critical for the no-penetration constraint in fluid-thin structure interaction problems.

In [35, Section 3], a numerical analysis of the original DAL was undertaken by introducing a scalar parabolic model problem with a Dirichlet boundary condition applied on a surface cutting through the interior of the domain. The analysis in [35] proceeded as follows: First, the model problem was related to a feedback forcing regularization. Second, the error was analyzed in discretizing this regularized problem in space and time. However, the dependence of the regularized problem's coefficients on refinement parameters introduced many technical difficulties into the analysis, and numerical experiments indicated that the resulting error bounds were not sharp.

The present paper aims to systematically address the accuracy for the projection-based DAL method by firstly addressing the solution regularity for the immersed thin solid problem and secondly providing the error estimates for the projection-based DAL method based on the regularity results. In [72] it was shown that for a homogeneous parabolic problem defined in a Lipschitz domain Ω, the initial boundary problem has a unique solution $u \in H^{3/4}(0,T;L^2(\Omega)) \cap L^2(0,T;H^{3/2}(\Omega))$. With the above results, we prove that, on a domain with an immersed Lipschitz surface, more regular initial condition and source terms lead to $u \in H^2(0,T;H^{3/2-\epsilon}(\Omega))$, and the normal jump of the gradient across the immersed interface is in $H^1(0,T;L^2(\Gamma))$ (see Theorem 4.2). We have also provided nearly-optimal estimates for the Dirichlet problem (see Lemma 5.3) and the Robin problem (see Lemma 5.5). Based on these regularity results, we develop the analysis of the projection-based DAL on the parabolic model problem, where the problem domain is separated into two subdomains by a Lipschitz surface of co-dimension one. The new analysis does not rely on passing through a regularized problem, and arrives at sharp bounds.

In this paper, we begin by reviewing the fluid–thin structure interaction problem setting (Section 2) and the immersogeometric FSI framework (Section 3) in which the DAL methods are developed and applied. Then, in Section 4, we recall the linear parabolic model problem introduced in [35, Section 3.1.1] and study the regularity of its solutions. Section 5 provides several critical lemmas and analyzes the convergence of the projection-based DAL method in the context of this model problem. Numerical testing in Section 6 supports the analysis on linear problems, and in Section 7 the numerical results on a novel benchmark 2D FSI problem indicate that the conclusions of the model problem analysis extrapolate to much more complicated problems. Section 8 summarizes our findings and discusses future research.

2. Mathematical model for FSI

This section defines the mathematical model of fluid–thin structure interaction for which the DAL methods we consider here were originally developed. We also outline the discretizations used for the fluid and thin structure subproblems.

2.1. *Augmented Lagrangian formulation of FSI*

We begin with a versatile augmented Lagrangian framework for FSI [73], which we specialize to the case of thin immersed structures. The region occupied by fluid is denoted $\Omega \subset \mathbb{R}^n$ where $n = 3$ or 2, and the deformed structure geometry at time t is modeled by the $n-1$ dimensional surface $\Gamma_t \subset \Omega$. Let $\mathbf{u}$ and p denote the fluid velocity and pressure fields. Let $\mathbf{y}$ denote the structure displacement relative to some reference configuration, Γ_0. The structure velocity is denoted $\boldsymbol{\eta} := \mathbf{y}_t$ which is the time derivative of $\mathbf{y}$. The fluid–structure kinematic constraint that $\mathbf{u} = \boldsymbol{\eta}$ on Γ_t is enforced using the augmented Lagrangian

$$\int_{\Gamma_t} \boldsymbol{\lambda} \cdot (\mathbf{u} - \boldsymbol{\eta})\, d\Gamma + \frac{1}{2} \int_{\Gamma_t} \beta |\mathbf{u} - \boldsymbol{\eta}|^2 \, d\Gamma \,, \tag{2.1}$$

in which $\boldsymbol{\lambda}$ is a Lagrange multiplier and $\beta \geq 0$ is a penalty parameter. This results in the following variational problem: Find $\mathbf{u} \in \mathcal{S}_u$, $p \in \mathcal{S}_p$, $\mathbf{y} \in \mathcal{S}_d$, and $\boldsymbol{\lambda} \in \mathcal{S}_\ell$ such that, for all $\mathbf{w}_1 \in \mathcal{V}_u$, $q \in \mathcal{V}_p$, $\mathbf{w}_2 \in \mathcal{V}_d$, and $\delta\boldsymbol{\lambda} \in \mathcal{V}_\ell$

$$B_1(\{\mathbf{u}, p\}, \{\mathbf{w}_1, q\}) - F_1(\{\mathbf{w}_1, q\}) + \int_{\Gamma_t} \mathbf{w}_1 \cdot \boldsymbol{\lambda}\, d\Gamma + \int_{\Gamma_t} \mathbf{w}_1 \cdot \beta(\mathbf{u} - \boldsymbol{\eta})\, d\Gamma \;=\; 0 \,, \tag{2.2}$$

$$B_2(\mathbf{y}, \mathbf{w}_2) - F_2(\mathbf{w}_2) - \int_{\Gamma_t} \mathbf{w}_2 \cdot \boldsymbol{\lambda}\, d\Gamma - \int_{\Gamma_t} \mathbf{w}_2 \cdot \beta(\mathbf{u} - \boldsymbol{\eta})\, d\Gamma \;=\; 0 \,, \tag{2.3}$$

$$\int_{\Gamma_t} \delta\boldsymbol{\lambda} \cdot (\mathbf{u} - \boldsymbol{\eta})\, d\Gamma \;=\; 0 \,, \tag{2.4}$$

where $\mathcal{S}_u$, $\mathcal{S}_p$, $\mathcal{S}_d$, and $\mathcal{S}_\ell$ are trial solution spaces for the different solution components and $\mathcal{V}_u$, $\mathcal{V}_p$, $\mathcal{V}_d$, and $\mathcal{V}_\ell$ are the corresponding test spaces. B_1, B_2, F_1, and F_2 are semi-linear forms and linear functionals defining the fluid and structure subproblems.

2.2. *Fluid subproblem*

We assume the fluid to be incompressible and Newtonian, with the following weak formulation

$$\begin{aligned} B_1(\{\mathbf{u}, p\}, \{\mathbf{w}, q\}) = &\int_\Omega \mathbf{w} \cdot \rho_f \left(\left.\frac{\partial \mathbf{u}}{\partial t}\right|_{\mathbf{x}} + \mathbf{u} \cdot \boldsymbol{\nabla}\mathbf{u} \right) d\Omega + \int_\Omega \boldsymbol{\varepsilon}(\mathbf{w}) : \boldsymbol{\sigma}_f \, d\Omega \\ &+ \int_\Omega q \boldsymbol{\nabla} \cdot \mathbf{u} \, d\Omega - \gamma \int_{\Gamma_N} \mathbf{w} \cdot \rho_f \left\{ \mathbf{u} \cdot \mathbf{n}_f \right\}_- \mathbf{u} \, d\Gamma \,, \end{aligned} \tag{2.5}$$

$$F_1(\{\mathbf{w}, q\}) = \int_\Omega \mathbf{w} \cdot \rho_f \mathbf{f}_1 \, d\Omega + \int_{\Gamma_N} \mathbf{w} \cdot \mathbf{T}_1 \, d\Gamma \,, \tag{2.6}$$

where ρ_1 is the mass density of the fluid, $\boldsymbol{\varepsilon}(\cdot)$ is the symmetric gradient, $\boldsymbol{\sigma}_f = -p\mathbf{I} + 2\mu\boldsymbol{\varepsilon}(\mathbf{u})$ is the fluid Cauchy stress, μ is the dynamic viscosity, $\mathbf{f}_1$ is a body force, $\mathbf{T}_1$ is a traction on $\Gamma_N \subset \partial\Omega$, and $\mathbf{n}_f$ is the unit outward-facing normal to Ω. $\partial(\cdot)/\partial t|_{\mathbf{x}}$ indicates time differentiation holding $\mathbf{x} \in \Omega$ fixed. In the last term of (2.5), the function $\{\cdot\}_-$ extracts the negative part of $(\cdot)$:

$$\{x\}_- = \begin{cases} 0 & x > 0 \\ x \text{ otherwise} \end{cases} \,. \tag{2.7}$$

This enhances the stability of the problem in situations where flow enters through Γ_N [35, 74]. The dimensionless coefficient γ controls the strength of stabilization.

Past work on immersogeometric analysis has discretized this subproblem in a number of ways. In [31], the variational multiscale (VMS) formulation is employed, with equal-order pressure and velocity interpolation. This suffered from difficulties with mass loss in the discrete fluid solution. In [35], this issue was circumvented by applying a modification of the divergence conforming (or div-conforming) discretization described in Evans and Hughes [75–77] and based on work by Buffa et al. [78, 79]. We refer interested readers to [75] for further information on div-conforming B-splines and [35, Section 2.2] for details of the implementation used for immersogeometric FSI analysis. Numerical FSI examples in this paper use the div-conforming fluid discretization.

2.3. *Thin structure subproblem*

We define the forms B_2 and F_2 for the structure subproblem by assuming Kirchhoff–Love thin shell kinematics [44, 80, 81]:

$$B_2(\mathbf{y}, \mathbf{w}) = \int_{\Gamma_t} \mathbf{w} \cdot \rho_s h_{\text{th}} \left.\frac{\partial^2 \mathbf{y}}{\partial t^2}\right|_{\mathbf{X}} d\Gamma + \int_{\Gamma_0} \int_{-h_{\text{th}}/2}^{h_{\text{th}}/2} D_{\mathbf{w}}\mathbf{E} : \mathbf{S}\, d\xi d\Gamma \tag{2.8}$$

and

$$F_2(\mathbf{w}) = \int_{\Gamma_t} \mathbf{w} \cdot \rho_s h_{\text{th}} \mathbf{f}_2\, d\Gamma + \int_{\Gamma_t} \mathbf{w} \cdot \mathbf{h}^{\text{net}}\, d\Gamma\,, \tag{2.9}$$

where ρ_s is mass density, $\mathbf{f}_2$ is a body force, h_{th} is the thickness of the shell, and ξ is a coordinate parameterizing the through-thickness direction. The elasticity term is referred to the reference configuration; $\mathbf{E}$ is the Green–Lagrange strain tensor,

$$D_{\mathbf{w}}\mathbf{E}(\mathbf{y}) = \left.\frac{d}{d\epsilon}\mathbf{E}(\mathbf{y} + \epsilon\mathbf{w})\right|_{\epsilon=0}\,, \tag{2.10}$$

and $\mathbf{S}$ is the second Piola–Kirchhoff stress tensor. The last term of F_2 combines tractions prescribed on both sides of Γ_t: $\mathbf{h}^{\text{net}} = \mathbf{h}(\xi = -h_{\text{th}}/2) + \mathbf{h}(\xi = +h_{\text{th}}/2)$. The time derivative $\partial(\cdot)/\partial t|_{\mathbf{X}}$ is taken holding $\mathbf{X} \in \Gamma_0$ fixed. $\mathbf{S}$ can be computed from $\mathbf{E}$ using an arbitrary constitutive model. Computing $\mathbf{E}$ from the midsurface displacement $\mathbf{y}$ relies on kinematic assumptions detailed in [44, 80, 81].

In the resulting thin shell subproblem, the smoothness of the solution space is especially important because of the high-order derivatives of $\mathbf{y}$ and $\mathbf{w}$ resulting from the mapping of $\mathbf{y}$ to $\mathbf{E}$. For $B_2(\mathbf{w}, \mathbf{y})$ to remain bounded, $\mathbf{w}$ and $\mathbf{y}$ must be at least in $H^2(\Gamma)$. Therefore, in this paper we employ isogeometric analysis (IGA) spline spaces to discretize the thin shell subproblem in space, because IGA accommodates the additional smoothness required of numerical solutions.

3. Projection-based dynamic augmented Lagrangian method

This section discusses how we discretize the constraint coupling the subproblems with the projection-based DAL method from [36]. In the immersogeometric framework of [31] the

constraint $\mathbf{u} = \boldsymbol{\eta}$ on Γ was formally separated into no-penetration and no-slip components:

$$\mathbf{u} \cdot \mathbf{n}_f = -\boldsymbol{\eta} \cdot \mathbf{n}_s, \tag{3.1}$$

$$\mathbf{u} - \Big(\mathbf{u} \cdot \mathbf{n}_f\Big)\mathbf{n}_f = \boldsymbol{\eta} - (\boldsymbol{\eta} \cdot \mathbf{n}_s)\,\mathbf{n}_s\,, \tag{3.2}$$

where $\mathbf{n}_s = -\mathbf{n}_f$. (3.1) and (3.2) are enforced by normal and tangential components of $\boldsymbol{\lambda}$, respectively, as well as the penalty forcing $\beta(\mathbf{u} - \boldsymbol{\eta})$. In the applications with a closed structure separating regions of different pressures (e.g. an aortic heart valve during diastole), the thin structure must be able to prevent leakage to maintain the correct qualitative solution behavior. On the other hand, the no-slip constraint is less essential; its strong enforcement may even be detrimental to solution quality on coarse meshes [82–85]. We therefore discretized these constraint components differently. For the no-slip constraint, we simply rely on imposing consistency with a penalty integral term and neglect the corresponding component of the Lagrange multiplier field. For the no-penetration constraint, we retain a scalar Lagrange multiplier field on Γ, denoted $\lambda = \boldsymbol{\lambda} \cdot \mathbf{n}_f$, to strengthen enforcement of non-penetration. Because Γ_t can cut through the fluid domain arbitrarily, it would be difficult to construct *inf-sup* stable combinations of discrete velocity and multiplier spaces. We discretize λ as a set of samples at quadrature points, which may be viewed as coefficients in a linear combination of piecewise-constant basis functions, each supported on the patch of surface area associated with a quadrature point (cf. similar interpretations of quadrature-point spaces in plasticity, e.g., [86, (6.6)–(6.7)] and [87, Remark 1].)

Since we do not place any upper bound on the density of quadrature points relative to the fluid and structure discretizations, no discrete *inf-sup* condition can be assumed. Although semi-implicit time integration can circumvent this in transient problems, the instability still manifests in the steady limit. Reference [34] introduced a regularized problem which perturbs the constraint by an amount controlled by the parameter $r \geq 0$. However, the perturbed constraint no longer satisfies the kinematic conservation law

$$\int_{\Gamma_t} (\mathbf{u} - \boldsymbol{\eta}) \cdot \mathbf{n}_f \, d\Gamma = 0\,, \tag{3.3}$$

which can only be recovered in the unstable limit of $r \to 0$. To stabilize the formulation while maintaining kinematic conservation, reference [36] introduced the projection operator P as an L^2 projection from $\mathcal{V}_\ell = L^2(\Gamma)$ to a finite-dimensional subspace $\mathcal{V}_H$: For $\lambda \in \mathcal{V}_\ell$,

$$\langle P\lambda, \delta\lambda \rangle = \langle \lambda, \delta\lambda \rangle\,, \qquad \forall \delta\lambda \in \mathcal{V}_H\,, \tag{3.4}$$

where $\langle \cdot, \cdot \rangle$ is the inner product in $L^2(\Gamma)$. The space $\mathcal{V}_H$ is defined on a coarse mesh of Γ, with element size $H > h$. In this paper, we keep $C \leq H/h$ where $C > 1$ is a sufficiently large constant required by the *inf-sup* condition, as will be discussed in Section 5. Practically, having $H \gg h$ as $h \to 0$ would be sufficient for the projection-based DAL method to converge. We also denote the complementary commutative projector of P as $P^\perp = I - P$, then we have,

$$\langle P\lambda, P^\perp \delta\lambda \rangle = \langle P^\perp \lambda, P\delta\lambda \rangle = 0\,, \qquad \forall \lambda,\, \delta\lambda \in \mathcal{V}_\ell\,. \tag{3.5}$$

With the coarse subspace $\mathcal{V}_H$ the projection-based immersogeometric framework can then be introduced by employing the spatial discretization as: Find $\mathbf{u} \in \mathcal{S}_u$, $p \in \mathcal{S}_p$, $\mathbf{y} \in \mathcal{S}_d$, and $\lambda \in \mathcal{V}_H$ such that, for all test functions $\mathbf{w}_1 \in \mathcal{V}_u$, $q \in \mathcal{V}_p$, $\mathbf{w}_2 \in \mathcal{V}_d$, and $\delta\lambda \in \mathcal{V}_H$

$$\begin{aligned} & B_1(\{\mathbf{w}_1, q\}, \{\mathbf{u}, p\}; \hat{\mathbf{u}}) - F_1(\{\mathbf{w}_1, q\}) + B_2(\mathbf{w}_2, \mathbf{y}) - F_2(\mathbf{w}_2) \\ & + \int_{\Gamma_t} (\mathbf{w}_1 - \mathbf{w}_2) \cdot \mathbf{n}_f \lambda \, d\Gamma + \int_{\Gamma_t} (\mathbf{w}_1 - \mathbf{w}_2) \cdot \tau^B_{\mathrm{NOR}} \left((\mathbf{u} - \boldsymbol{\eta}) \cdot \mathbf{n}_f \right) \mathbf{n}_f \, d\Gamma \\ & + \int_{\Gamma_t} (\mathbf{w}_1 - \mathbf{w}_2) \cdot \tau^B_{\mathrm{TAN}} \left((\mathbf{u} - \boldsymbol{\eta}) - \left((\mathbf{u} - \boldsymbol{\eta}) \cdot \mathbf{n}_f \right) \mathbf{n}_f \right) \, d\Gamma \\ & + \int_{\Gamma_t} \delta\lambda (\mathbf{u} - \boldsymbol{\eta}) \cdot \mathbf{n}_f \, d\Gamma \; = \; 0 \, . \end{aligned} \tag{3.6}$$

Applying spatial discretizations to the subproblems of (3.6), as discussed in previous sections, allows us to represent the semi-discrete solutions as vectors of basis function coefficients, which is convenient for discussing time integration algorithms. When describing time stepping procedures for the fully-discrete problem, we use n to denote the time step index, and denote the spatiallydiscretized fluid velocity solution as a vector of basis function coefficients $\mathbf{U}^n$. Likewise, the spatially discretized fluid velocity time derivative, fluid pressure, structure displacement, and displacement time derivatives are denoted $\dot{\mathbf{U}}^n$, $\mathbf{P}^n$, $\mathbf{Y}^n$, $\dot{\mathbf{Y}}^n$, and $\ddot{\mathbf{Y}}^n$. We denote the discretized multiplier at time level n as Λ^n.

The time discretization proposed in [31, 34] proceeds in two phases at each time step. First, Λ is held fixed at Λ^n, and the penalty-coupled problem is solved implicitly. Second, Λ^{n+1} is computed explicitly. More precisely, the algorithm of [31, 34] considered solution variables at time level n known, and first solved the following problem for all $(n+1)$-level unknowns except Λ^{n+1}:

$$\mathrm{Res}\left(\mathbf{U}^{n+\alpha_f}, \dot{\mathbf{U}}^{n+\alpha_m}, \mathbf{Y}^{n+\alpha_f}, \dot{\mathbf{Y}}^{n+\alpha_f}, \ddot{\mathbf{Y}}^{n+\alpha_m}, \mathbf{P}^{n+1}, \Lambda^n \right) = \mathbf{0} \, , \tag{3.7}$$

$$\mathbf{U}^{n+1} = \mathbf{U}^n + \Delta t \left((1-\gamma) \dot{\mathbf{U}}^n + \gamma \dot{\mathbf{U}}^{n+1} \right) \, , \tag{3.8}$$

$$\dot{\mathbf{U}}^{n+\alpha_m} = \dot{\mathbf{U}}^n + \alpha_m \left(\dot{\mathbf{U}}^{n+1} - \dot{\mathbf{U}}^n \right) \, , \tag{3.9}$$

$$\mathbf{U}^{n+\alpha_f} = \mathbf{U}^n + \alpha_f \left(\mathbf{U}^{n+1} - \mathbf{U}^n \right) \, , \tag{3.10}$$

$$\mathbf{Y}^{n+1} = \mathbf{Y}^n + \Delta t \dot{\mathbf{Y}}^n + \frac{\Delta t^2}{2} \left((1-2\beta) \ddot{\mathbf{Y}}^n + 2\beta \ddot{\mathbf{Y}}^{n+1} \right) \, , \tag{3.11}$$

$$\dot{\mathbf{Y}}^{n+1} = \dot{\mathbf{Y}}^n + \Delta t \left((1-\gamma) \ddot{\mathbf{Y}}^n + \gamma \ddot{\mathbf{Y}}^{n+1} \right) \, , \tag{3.12}$$

$$\ddot{\mathbf{Y}}^{n+\alpha_m} = \ddot{\mathbf{Y}}^n + \alpha_m \left(\ddot{\mathbf{Y}}^{n+1} - \ddot{\mathbf{Y}}^n \right) \, , \tag{3.13}$$

$$\dot{\mathbf{Y}}^{n+\alpha_f} = \dot{\mathbf{Y}}^n + \alpha_f \left(\dot{\mathbf{Y}}^{n+1} - \dot{\mathbf{Y}}^n \right) \, , \tag{3.14}$$

$$\mathbf{Y}^{n+\alpha_f} = \mathbf{Y}^n + \alpha_f \left(\mathbf{Y}^{n+1} - \mathbf{Y}^n \right) \, , \tag{3.15}$$

where α_m, α_f, β, and γ are time integration parameters. Δt is the time step size. Res(...) is the nonlinear algebraic residual corresponding to discretization of (3.6) with Λ fixed and $\mathcal{V}_H = \emptyset$. The subproblems are still coupled through the penalty term, but in a more gentle way, which can be resolved using block iteration [35, Section 4]. Equations (3.7)–(3.15) come from the generalized-α method of time integration [88]. In [31–34], the authors

followed [89, Section 4.4] by using a subset of generalized-α methods parameterized by $\rho_\infty \in [0, 1]$, which controls numerical damping and defines the four free parameters as

$$\alpha_m = \frac{1}{2}\left(\frac{3-\rho_\infty}{1+\rho_\infty}\right), \alpha_f = \frac{1}{1+\rho_\infty}, \gamma = \frac{1}{2} + \alpha_m - \alpha_f, \beta = \frac{1}{4}\left(1 + \alpha_m - \alpha_f\right)^2. \quad (3.16)$$

The mathematical interpretation of ρ_∞ is it is the spectral radius of the amplification matrix as $\Delta t \to \infty$; see [88]. In FSI examples within this work, we maintain a direct analogy to the linear model problems analyzed in Section 5 by using the backward Euler method instead. This can be conveniently implemented within the generalized-α predictor–multi-corrector scheme of [89] by setting the generalized-α parameters to $\alpha_m = \alpha_f = \gamma = \beta = 1$ and modifying the displacement predictor to be consistent with the backward Euler method.

The second, explicit phase of the projection-based DAL time stepping procedure is to update the Lagrange multiplier:

$$\Lambda^{n+1} \leftarrow P\left(\Lambda^n + \tau^B_{\mathrm{NOR}}\left(\mathbf{u}^{n+\alpha_f} - \eta^{n+\alpha_f}\right) \cdot \mathbf{n}_f^{n+\alpha_f}\right). \quad (3.17)$$

Summarizing, then, the projection-based DAL method uses the following two-phase time stepping procedure:

(1) Solve (3.7)–(3.15) with Λ^n fixed.
(2) Update Λ^{n+1} by (3.17).

For general $\mathcal{V}_H$, the second step would require inverting a matrix. However, this step can be made explicit by considering $\mathcal{V}_H$ to consist of piecewise constants on the elements of the coarse boundary mesh, rendering the projection matrix diagonal.

Regarding the choices of the penalty parameters, it was suggested, based on dimensional analysis and physical considerations [35, Section 5.2.1], to set

$$\tau^B_{\mathrm{TAN}} = C_{\mathrm{TAN}}\frac{\mu}{h} \text{ and } \tau^B_{\mathrm{NOR}} = \max\left\{C^{\mathrm{inert}}_{\mathrm{NOR}}\frac{\rho_1 h}{\Delta t}, C^{\mathrm{visc}}_{\mathrm{NOR}}\frac{\mu}{h}\right\}, \quad (3.18)$$

where C_{TAN}, $C^{\mathrm{inert}}_{\mathrm{NOR}}$, and $C^{\mathrm{visc}}_{\mathrm{NOR}}$ are dimensionless $O(1)$ constants and h is the fluid element diameter. When analyzing this projection-based DAL method for the linear parabolic problem in Section 5, we consider the normal penalty only and take the asymptotic value of the parameter as $\tau^B_{\mathrm{NOR}} = \beta = O(1/h)$.

4. A model problem and its regularity

To develop error estimates for the projection-based DAL, we formulate this method for a linear model problem in a domain with finite diameter, as shown in Figure 1. Specifically, we assume that there the Dirichlet condition is imposed in an immersed surface which fully separates the domain Ω into two Lipschitz subdomains Ω_1 and Ω_2. Therefore, both the immersed surface as well as the domain boundary are Lipschitz continuous. We note that the domain in Figure 1 can be seen as an analog of the fluid problem in the heart valve application when the valve is fully closed. To ensure general applicability of the derived error estimates, we first provide analysis of the regularity of solutions to this model

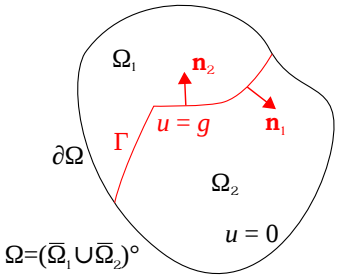

Fig. 1. The Lipschitz domain $\Omega = (\overline{\Omega}_1 \cup \overline{\Omega}_2)^\circ$ and the immersed boundary Γ.

problem. In this section, for each variable b defined on the whole domain Ω, we use b_i to denote $b|_{\Omega_i}$, where $i = 1$ or 2.

On the domain as defined in Figure 1, a parabolic interface problem is considered: Given $u_0(\mathbf{x}) \in C^4(\Omega)$, $f(\mathbf{x}, t) \in L^2(\Omega \times (0, T))$ with $f_i = f|_{\Omega_i}$ in $C^2(\Omega_i \times (0, T))$, and the boundary condition $g(\mathbf{x}, t) \in C^3(0, T; H_0^1(\Gamma))$, assuming that Ω_i is a Lipschitz regular domain for both $i = 1$ and 2, find $u = u(\mathbf{x}, t)$ satisfying

$$\frac{\partial u_i}{\partial t} - \nabla \cdot c(\nabla u_i) = f_i(\mathbf{x}, t), \quad \text{in } \Omega_i \times (0, T)\ ,\ i \in \{1, 2\}, \tag{4.1a}$$

$$u(\mathbf{x}, t) = g(\mathbf{x}, t), \quad \text{on } \Gamma \times (0, T), \tag{4.1b}$$

$$u(\mathbf{x}, 0) = u_0(\mathbf{x}), \quad \text{in } \Omega, \tag{4.1c}$$

$$u(\mathbf{x}, t) = 0, \quad \text{on } \partial\Omega \times (0, T). \tag{4.1d}$$

Here Ω, Ω_i, and Γ are shown in Figure 1; c is a linear transformation that we further consider to be multiplication by a constant, $c(\mathbf{v}) = \kappa\mathbf{v}$, and $g(\mathbf{x}, t)$ can be seen as analogous to the shell structure velocity. Note that the isogeometric analysis (IGA) spline spaces are employed in the thin shell subproblem, which can accommodate the regularity requirement of $g(\mathbf{x}, t)$ here. In the thin structure problem, the fluid pressure is not continuous across the thin structure, and the second spatial derivative of fluid velocity is not well-defined on the interface. Here we note that problem (4.1) can be seen as "gluing" two subproblems on Ω_1 and Ω_2 together. However, in the immersogeometric problem we are actually solving for the solution on the whole domain Ω. Therefore, we state a problem for u without reference to the subdomains by re-writing the problem in a weak formulation, in which we introduce the Lagrange multiplier $\lambda = -c(\nabla u_1) \cdot \mathbf{n}_1 - c(\nabla u_2) \cdot \mathbf{n}_2$:

$$\left(\frac{\partial u}{\partial t}, v\right) + a(u, v) + \langle \lambda, v \rangle = (f, v), \quad \text{for all test functions } v \in X, \tag{4.2a}$$

$$\langle u, \delta\lambda \rangle = \langle g, \delta\lambda \rangle, \quad \text{for all test functions } \delta\lambda \in M, \tag{4.2b}$$

$$u(\mathbf{x}, 0) = u_0(\mathbf{x}), \quad \text{in } \Omega, \tag{4.2c}$$

$$u(\mathbf{x}, t) = 0, \quad \text{on } \partial\Omega \times (0, T). \tag{4.2d}$$

Here $(\cdot, \cdot)$ and $\langle \cdot, \cdot \rangle$ denote the inner product in $L^2(\Omega)$ and in $L^2(\Gamma)$, respectively. $X = H_0^1(\Omega)$, $M = H_{00}^{-1/2}(\Gamma)$ is the dual space of $H_{00}^{1/2}(\Gamma) = \{\delta\gamma \in H^{1/2}(\Gamma) :$ the extension by zero of $\delta\gamma \in$

$H^{1/2}(\partial\Omega_i)$ for $i = 1, 2\}$, and the bilinear operator $a(u, v) := \int_\Omega c(\nabla u) \cdot \nabla v$ is elliptic, i.e., $a(u, u) = \kappa\|\nabla u\|^2_{L^2(\Omega)}$, and continuous, i.e., $a(u, v) \le \kappa\|\nabla u\|_{L^2(\Omega)}\|\nabla v\|_{L^2(\Omega)}$.

The regularity results are mainly given by the following result due to Mitrea [72, Theorem 9.1], which we apply here in the Euclidean setting (instead of the more general Riemannian manifold setting):

Theorem 4.1. *Let L be a second order, self-adjoint, strongly elliptic operator with smooth coefficients. D is a Lipschitz regular domain with finite diameter (diam $D < \infty$). When the boundary condition $h(\mathbf{x}, t)$ is in $L^2_{1,1/2}(\partial D \times (0, T))$, the homogeneous parabolic problem*

$$\begin{aligned} &\frac{\partial u}{\partial t} + Lu = 0, \quad \text{in } D \times (0, T), \\ &u(\mathbf{x}, t) = h(\mathbf{x}, t), \quad \text{on } \partial D \times (0, T), \\ &u(\mathbf{x}, 0) = 0 \quad \text{in } D, \end{aligned}$$

admits a solution $u \in H^{3/4}(0, T; L^2(D)) \cap L^2(0, T; H^{3/2}(D))$. Here $f \in L^2_{1,1/2}(\partial D \times (0, T))$ means both $\nabla_{tan} f$ and $D_t^{1/2} f$ belong to $L^2(\partial D \times (0, T))$.

We remark that although this theorem is stated for homogeneous equations $\frac{\partial u}{\partial t} + Lu = 0$, it can be easily generalized (in the same way as for the heat equation) to inhomogeneous equations of the form $\frac{\partial u}{\partial t} + Lu = f$ with regular functions f.

Since c is a linear transformation, the operator $Lu := -\nabla \cdot c(\nabla u)$ given by

$$\langle Lu, v\rangle := \int_\Omega c(\nabla u) \cdot \nabla v d\mathbf{x} \qquad \text{for all test functions } v,$$

is strongly elliptic and satisfies the conditions in Theorem 4.1. With the above theorem, we can then obtain the regularity of problem (4.2), for $\Omega \in \mathbb{R}^2$ and $\Omega \in \mathbb{R}^3$:

Theorem 4.2. *For $\Omega \in \mathbb{R}^n$ ($n = 2$ or 3) with finite diameter (diam $\Omega < \infty$), when Ω_i ($i = 1, 2$) are both Lipschitz regular domains, a sufficiently regular initial datum $u_0 \in C^4(\Omega)$, the force loading $f(\mathbf{x}, t)$ is in $L^2(\Omega \times (0, T))$ and $f_i = f|_{\Omega_i}$ is in $C^2(\Omega_i \times (0, T))$, and the boundary condition $g(\mathbf{x}, t)$ is in $C^3(0, T; H^1_0(\Gamma))$, the solutions $u_i(\mathbf{x}, t)$ ($i = 1, 2$) of the parabolic problem (4.2) have regularity $H^2(0, T; H^{3/2}(\Omega_i))$ and therefore the solution $u(\mathbf{x}, t)$ has regularity $H^2(0, T; H^{3/2-\epsilon}(\Omega))$. Moreover, the Lagrange multiplier $\lambda = -c(\nabla u_1) \cdot \mathbf{n}_1 - c(\nabla u_2) \cdot \mathbf{n}_2$ has regularity $H^1(0, T; L^2(\Gamma))$.*

Proof. We first consider the case when the right derivative $\left.\frac{\partial^2 u}{\partial t^2}\right|_{t=0^+} = 0$. Let $\tilde{f} := f - v_0 -$

$tLv_0 - Lu_0$, $\tilde{g} := g - tv_0|_\Gamma - u_0|_\Gamma$ where $v_0 = \left.\dfrac{\partial u}{\partial t}\right|_{t=0^+}$, and consider

$$\frac{\partial w_i}{\partial t} - \nabla \cdot c(\nabla w_i) = \frac{\partial^2 f}{\partial t^2}, \quad \text{in } \Omega_i \times (0,T), \tag{4.3a}$$

$$w_i = \frac{\partial^2 g}{\partial t^2}, \quad \text{on } \Gamma\times(0,T), \tag{4.3b}$$

$$w_i = 0, \quad \text{on } \partial\Omega \times (0,T), \tag{4.3c}$$

$$w_i(\mathbf{x},0) = 0, \quad \text{in } \Omega_i. \tag{4.3d}$$

With Theorem 4.1 we can see that (4.3) admits a solution $w_i(\mathbf{x},t) \in L^2(0,T;H^{3/2}(\Omega_i))$. Here we remark that the regularity in space $H^{3/2}(\Omega_i)$ is insufficient to ensure that $\nabla \cdot c(\nabla w_i)$ is well defined as a function. Similarly, the regularity in time is also insufficient to ensure $\dfrac{\partial w_i}{\partial t}$ is well defined as a function. Thus the solution w_i is to be interpreted in the weak sense, i.e.

$$\int_{\Omega_i} \left(\frac{\partial w_i}{\partial t} - \nabla \cdot c(\nabla w_i) \right) \varphi d\mathbf{x} := \int_{\Omega_i} \left(-w_i \frac{\partial \varphi}{\partial t} + a(w_i, \varphi) \right) d\mathbf{x} = \int_{\Omega_i} \frac{\partial^2 f}{\partial t^2} \varphi d\mathbf{x}$$

for a.e. time $t \in (0,T)$, and all test functions $\varphi \in C_c^\infty(\Omega_i \times (0,T))$.

Now consider an antiderivative (in time) v_i of w_i given by

$$v_i(\mathbf{x},t) := \int_0^t w_i(\mathbf{x},s)ds + v_0(\mathbf{x}),$$

with a sufficiently regular v_0 (e.g. $v_0 \in C^4(\Omega)$). Note that $v_i \in H^1(0,T;H^{3/2}(\Omega_i))$ is the solution of

$$\frac{\partial v_i}{\partial t} - \nabla \cdot c(\nabla v_i) = \frac{\partial \tilde{f}}{\partial t} + Lv_0(\mathbf{x}) = \frac{\partial f}{\partial t}, \quad \text{in } \Omega_i \times (0,T), \tag{4.4a}$$

$$v_i = \frac{\partial \tilde{g}}{\partial t} + v_0|_\Gamma(\mathbf{x}) = \frac{\partial g}{\partial t}, \quad \text{on } \Gamma\times(0,T), \tag{4.4b}$$

$$v_i = 0, \quad \text{on } \partial\Omega \times (0,T), \tag{4.4c}$$

$$v_i(\mathbf{x},0) = v_0(\mathbf{x}), \quad \text{in } \Omega_i. \tag{4.4d}$$

Finally consider an antiderivative (in time) u_i of v_i given by

$$u_i(\mathbf{x},t) := \int_0^t \int_0^s w_i(\mathbf{x},s')ds'ds + tv_0(\mathbf{x}) + u_0(\mathbf{x}).$$

Note that $u_i \in H^2(0,T;H^{3/2}(\Omega_i))$ is the solution of

$$\frac{\partial u_i}{\partial t} - \nabla \cdot c(\nabla u_i) = \tilde{f}(\mathbf{x},t) + v_0(\mathbf{x}) + tLv_0(\mathbf{x}) + Lu_0(\mathbf{x}) = f(\mathbf{x},t), \quad \text{in } \Omega_i \times (0,T), \tag{4.5a}$$

$$u_i = \tilde{g}(\mathbf{x},t) + tv_0|_\Gamma(\mathbf{x}) + u_0|_\Gamma(\mathbf{x}) = g(\mathbf{x},t), \quad \text{on } \Gamma\times(0,T), \tag{4.5b}$$

$$u_i = 0, \quad \text{on } \partial\Omega \times (0,T), \tag{4.5c}$$

$$u_i(\mathbf{x},0) = u_0(\mathbf{x}), \quad \text{in } \Omega_i. \tag{4.5d}$$

Note that all u_i, v_i, w_i are $H^{3/2}$ regular in space, in both Ω_1 and Ω_2.

The function u is then obtained by "gluing" together u_i. So $u|_{\Omega_i} = u_i$, and we need to check that $u \in H^{3/2-\epsilon}(\Omega)$. Firstly $u \in H^1(\Omega)$ is obvious. We then just need to check the Gagliardo seminorm $[\nabla u]_{1/2-\epsilon}$ is finite. Let $\widetilde{\nabla u_i}$ be the extensions to zero of ∇u_i outside Ω_i. Since $\nabla u_i \in H^{1/2-\epsilon}(\Omega_i)$, by extending to zero we have $\widetilde{\nabla u_i} \in H^{1/2-\epsilon}(\Omega)$ (cf, [90, Theorem 11.4]). Then for any test function $\varphi \in C_0^\infty(\Omega)$ we have

$$\int_\Omega (\widetilde{\nabla u_1} + \widetilde{\nabla u_2}) \cdot \varphi d\mathbf{x} = \int_{\Omega_1} \widetilde{\nabla u_1} \cdot \varphi d\mathbf{x} + \int_{\Omega_2} \widetilde{\nabla u_2} \cdot \varphi d\mathbf{x} = \int_{\Omega_1} \nabla u_1 \cdot \varphi d\mathbf{x} + \int_{\Omega_2} \nabla u_2 \cdot \varphi d\mathbf{x}$$

and by integration by parts

$$\begin{aligned}
\int_{\Omega_1} \nabla u_1 \cdot \varphi d\mathbf{x} &= \int_{\partial\Omega_1} u_1 \varphi \cdot \mathbf{n}_1 ds - \int_{\Omega_1} u_1 \nabla \cdot \varphi d\mathbf{x}, \\
\int_{\Omega_2} \nabla u_2 \cdot \varphi d\mathbf{x} &= \int_{\partial\Omega_2} u_2 \varphi \cdot \mathbf{n}_2 ds - \int_{\Omega_2} u_2 \nabla \cdot \varphi d\mathbf{x},
\end{aligned}$$

thus

$$\begin{aligned}
\int_\Omega (\widetilde{\nabla u_1} + \widetilde{\nabla u_2}) \cdot \varphi d\mathbf{x} &= \int_{\partial\Omega_1} u_1 \varphi \cdot \mathbf{n}_1 ds + \int_{\partial\Omega_2} u_2 \varphi \cdot \mathbf{n}_2 ds - \int_\Omega u \nabla \cdot \varphi d\mathbf{x} \\
&= -\int_\Omega u \nabla \cdot \varphi d\mathbf{x} = \int_\Omega \nabla u \cdot \varphi d\mathbf{x} - \int_{\partial\Omega} u\varphi \cdot \mathbf{n} ds, \qquad (4.6)
\end{aligned}$$

where

$$\int_{\partial\Omega_1} u_1 \varphi \cdot \mathbf{n}_1 ds + \int_{\partial\Omega_2} u_2 \varphi \cdot \mathbf{n}_2 ds = \int_{\partial\Omega} u\varphi \cdot \mathbf{n} ds = 0$$

since $u_1 = u_2$, $\mathbf{n}_1 = -\mathbf{n}_2$ on Γ and $\varphi = 0$ on $\partial\Omega$. Thus $\nabla u = \widetilde{\nabla u_1} + \widetilde{\nabla u_2} \in H^{1/2-\epsilon}(\Omega)$ and $u \in H^{3/2-\epsilon}(\Omega)$. Note that here the classical integration by parts formula can be applied to $H^1(\Omega_i)$ functions u_i, where restrictions to $\partial\Omega_i$ are understood in the usual trace sense.

Thus $u = u_1 + u_2$ (solution of (4.2)), satisfies $u \in H^2(0, T; H^{3/2-\epsilon}(\Omega))$. Moreover, at all times $s \in [0, T)$, the right derivative $\left.\dfrac{\partial^2 u}{\partial t^2}\right|_{t=s^+}$ is well-defined.

Note that in the above construction, as soon as we fix the inhomogeneous term in the equation for u_i (i.e. $\dfrac{\partial u_i}{\partial t} - \nabla \cdot c(\nabla u_i) = f$), then the inhomogeneous term in the equations for v_i and w_i are both fixed. This is expected since v_i, w_i can be seen as the time derivatives of u_i, thus the inhomogeneous term in the heat equations for v_i and w_i must be related to the inhomogeneous term in heat equation of u_i. Now we consider the case $w(\mathbf{x}, 0) = w_0(\mathbf{x}) = \left.\dfrac{\partial^2 u}{\partial t^2}\right|_{t=0^+} \neq 0$. We replace the functions f and g in (4.3), (4.4) and (4.5) with $F := f - tw_0 - \dfrac{t^2}{2} L w_0$ and $G := g - \dfrac{t^2}{2} w_0|_\Gamma$, and let $\hat{w}_i, \hat{v}_i, \hat{u}_i$ denote the solutions of the new (4.3), (4.4) and (4.5) respectively. Set $u_i := \hat{u}_i + \dfrac{t^2}{2} w_0$, $v_i := \hat{v}_i + tw_0$, and $w_i := \hat{w}_i + w_0$,

then u_i is the solution of

$$\begin{aligned}\frac{\partial u_i}{\partial t} - \nabla \cdot c(\nabla u_i) = F(\mathbf{x},t) + tw_0 + \frac{t^2}{2}Lw_0 = f(\mathbf{x},t), \quad \text{in } \Omega_i \times (0,T),\\ u_i = G(\mathbf{x},t) + \frac{t^2}{2}w_0|_\Gamma = g(\mathbf{x},t), \quad \text{on } \Gamma\times(0,T),\\ u_i = 0, \quad \text{on } \partial\Omega \times (0,T),\\ u_i(\mathbf{x},0) = u_0(\mathbf{x}), \quad \text{in } \Omega_i,\end{aligned}$$

v_i is the solution of

$$\begin{aligned}\frac{\partial v_i}{\partial t} - \nabla \cdot c(\nabla v_i) = \frac{\partial F}{\partial t} + w_0 + tLw_0, \quad \text{in } \Omega_i \times (0,T),\\ v_i = \frac{\partial G}{\partial t} + tw_0|_\Gamma, \quad \text{on } \Gamma \times (0,T),\\ v_i = 0, \quad \text{on } \partial\Omega \times (0,T),\\ v_i(\mathbf{x},0) = v_0(\mathbf{x}), \quad \text{in } \Omega_i,\end{aligned}$$

and w_i is then solution of

$$\begin{aligned}\frac{\partial w_i}{\partial t} - \nabla \cdot c(\nabla w_i) = \frac{\partial^2 F}{\partial t^2} + Lw_0, \quad \text{in } \Omega_i \times (0,T),\\ w_i = \frac{\partial^2 G}{\partial t^2} + w_0|_\Gamma(\mathbf{x}), \quad \text{on } \Gamma\times(0,T),\\ w_i = 0, \quad \text{on } \partial\Omega \times (0,T),\\ w_i(\mathbf{x},0) = w_0(\mathbf{x}), \quad \text{in } \Omega_i.\end{aligned}$$

Applying the same arguments of extension used to obtain $u \in H^2(0,T;H^{3/2-\epsilon}(\Omega))$ would give $v = v_1 + v_2 \in H^1(0,T;H^{3/2-\epsilon}(\Omega))$ and $w = w_1 + w_2 \in L^2(0,T;H^{3/2-\epsilon}(\Omega))$. Finally, since we have sufficient regularity on the boundary function g to apply Equations (9.4) and (9.5) of [72, Theorem 9.1], the Lagrange multiplier $\lambda = -c(\nabla u_1)\cdot \mathbf{n}_1 - c(\nabla u_2)\cdot \mathbf{n}_2$ has regularity $H^1(0,T;L^2(\Gamma))$. □

Remark 4.1. If one replaces the $\nabla \cdot c(\nabla u) = \kappa\Delta u$ operator with any strongly elliptic operator L with smooth coefficients, the solutions $u_i = u|_{\Omega_i}$ will have degraded regularity $u_i \in H^2(0,T;H^{3/2-\epsilon}(\Omega_i))$ but the conclusion $u \in H^2(0,T;H^{3/2-\epsilon}(\Omega))$ still holds.

5. Convergence of the projection-based DAL method

In this section, we aim to estimate, *a priori*, the error for the projection-based DAL method introduced in Section 3, when applied to the problem given in Section 4. The spatial error for an elliptic interface problem is estimated in Section 5.1, and the error of a fully discretized scheme for a parabolic interface problem is provided in Section 5.2. Throughout this section, we consider the symbol "C" to indicate a generic constant that is independent

of h, H, and Δt, but may have different numerical values in different situations. Although in Theorem 4.2 the regularity result $u \in H^2(0,T;H^{3/2-\epsilon}(\Omega))$ applies for any $\epsilon > 0$, in this section we further restrict the range of ϵ to $0 < \epsilon \ll \frac{1}{2}$ for the error estimates.

For the projection-based DAL method, introducing the Lagrange multiplier $\lambda = -(c(\nabla u_1)\cdot \mathbf{n}_1 + c(\nabla u_2)\cdot \mathbf{n}_2)$ yields an alternative weak formulation for this interface problem, as shown in (4.2). To state the numerical method, we associate with Ω a regular quasi-uniform triangulation $\mathcal{T}_h(\Omega)$ consisting of elements T of mesh sizes $h = \max_{\mathcal{T}_h(\Omega)} h_T$. The low regularity of the solution to the model problem implies that the minimum distance between u and a discrete solution on an unfitted mesh will converge at low order, so, for simplicity, we assume that the space X is approximated by continuous linear finite elements, viz.

$$X_h(\Omega) = \{w_h \in P_1(T) \mid w_h = 0 \text{ on } \partial\Omega\} \ . \tag{5.1}$$

Let $W_h(\Gamma)$ be the restriction of $X_h(\Omega)$ to Γ. For the projection, we consider a coarse, piecewise constant function space $W_H(\Gamma)$ on the interface, which may have jump discontinuities at element boundaries. Γ is associated with a regular quasi-uniform triangulation $\mathcal{K}_H(\Gamma)$ with mesh size $H := \max_{\mathcal{K}_H(\Gamma)} H_K$ and the space W is approximated by discontinuous piecewise constant elements, viz.

$$W_H(\Gamma) = \{\delta\lambda_H \in P_0(K)\} \ . \tag{5.2}$$

We further assume that $X_h(\Omega)$ and $W_H(\Gamma)$ are both strongly regular [91]. The Lagrange multiplier method with projection-based stabilization technique in Section 3 can now be applied on the weak problem (4.2): Find $(u_h^{n+1}, \lambda_H^{n+1}) \in X_h \times W_H$ such that for all $w_h \in X_h$ and $\delta\lambda_H \in W_H$,

$$\left(\frac{u_h^{n+1}-u_h^n}{\Delta t}, w_h\right) + a(u_h^{n+1}, w_h) + \langle \lambda_H^n, w_h\rangle + \beta\left\langle u_h^{n+1} - g(t^{n+1}), w_h\right\rangle = (f(t^{n+1}), w_h), \tag{5.3a}$$

$$\left\langle \lambda_H^{n+1}, \delta\lambda_H\right\rangle = \langle \lambda_H^n, \delta\lambda_H\rangle + \beta\left\langle P(u_h^{n+1} - g(t^{n+1})), \delta\lambda_H\right\rangle \ . \tag{5.3b}$$

From (5.3b) and the orthogonality property of the projection operator P onto W_H, taking $\delta\lambda = w_h|_\Gamma$ we have

$$\begin{aligned}\left\langle \lambda_H^{n+1}, w_h\right\rangle &= \langle \lambda_H^n, P(w_h)\rangle + \beta\left\langle P\left(u_h^{n+1} - g\left(t^{n+1}\right)\right), P(w_h)\right\rangle \\ &= \langle \lambda_H^n, w_h\rangle + \beta\left\langle u_h^{n+1} - g\left(t^{n+1}\right), w_h\right\rangle - \beta\left\langle P^\perp\left(u_h^{n+1} - g\left(t^{n+1}\right)\right), P^\perp(w_h)\right\rangle \ .\end{aligned}$$

Substituting into (5.3a) yields

$$\begin{aligned}&\left(\frac{u_h^{n+1}-u_h^n}{\Delta t}, w_h\right) + a\left(u_h^{n+1}, w_h\right) + \left\langle \lambda_H^{n+1}, P(w_h)\right\rangle + \beta\left\langle P^\perp\left(u_h^{n+1}\right), P^\perp(w_h)\right\rangle \\ &= \left(f(t^{n+1}), w_h\right) + \beta\left\langle P^\perp\left(g\left(t^{n+1}\right)\right), P^\perp(w_h)\right\rangle \ ,\end{aligned} \tag{5.4}$$

and (5.3b) can be written as

$$\Delta t\left\langle \frac{\lambda_H^{n+1}-\lambda_H^n}{\Delta t}, \delta\lambda_H\right\rangle = \beta\left\langle P\left(u_h^{n+1} - g\left(t^{n+1}\right)\right), \delta\lambda_H\right\rangle \ . \tag{5.5}$$

Combining (5.4) with (5.5) with $\delta\lambda_H = P(w_h|_\Gamma)$ we can obtain

$$\left(\frac{u_h^{n+1}-u_h^n}{\Delta t}, w_h\right) - \Delta t\left\langle\frac{\lambda_H^{n+1}-\lambda_H^n}{\Delta t}, w_h\right\rangle + a(u_h^{n+1}, w_h) + \left\langle\lambda_H^{n+1}, P(w_h)\right\rangle + \beta\left\langle u_h^{n+1}, w_h\right\rangle$$
$$= \left(f\left(t^{n+1}\right), w_h\right) + \beta\left\langle g\left(t^{n+1}\right), w_h\right\rangle , \tag{5.6}$$

In the following derivations, we will use the mesh-dependent half norm on Γ based on the mesh X_h

$$\|\lambda\|_{1/2,h}^2 = \frac{1}{h}\langle\lambda,\lambda\rangle , \qquad \|\lambda\|_{-1/2,h}^2 = h\langle\lambda,\lambda\rangle. \tag{5.7}$$

5.1. *Static: Elliptic interface problem*

We first study the error estimate for the static problem

$$a(u,w) + \langle\lambda, w\rangle = (f,w), \quad \forall w \in X, \tag{5.8a}$$
$$\langle u - g, \delta\lambda\rangle = 0, \qquad \forall\delta\lambda \in M. \tag{5.8b}$$

The steady limit of the projection-based DAL method can be written as

$$a(u_h, w_h) + \langle\lambda_H, w_h\rangle + \beta\langle u_h, w_h\rangle = (f, w_h) + \beta\langle g, w_h\rangle , \quad \forall w_h \in X_h \tag{5.9a}$$
$$\langle u_h - g, \delta\lambda_H\rangle = 0 , \quad \forall\delta\lambda_H \in W_H . \tag{5.9b}$$

Defining

$$\mathcal{A}(u_h, \lambda_H; w_h, \delta\lambda_H) = a(u_h, w_h) + \langle\lambda_H, w_h\rangle - \langle u_h, \delta\lambda_H\rangle + \beta\langle u_h, w_h\rangle \tag{5.10}$$

and

$$\mathcal{F}(w_h, \delta\lambda_H) = (f, w_h) - \langle g, \delta\lambda_H\rangle + \beta\langle g, w_h\rangle , \tag{5.11}$$

the formulation (5.9) can be written as

$$\mathcal{A}(u_h, \lambda_H; w_h, \delta\lambda_H) = \mathcal{F}(w_h, \delta\lambda_H), \quad \forall w_h \in X_h, \delta\lambda_H \in W_H. \tag{5.12}$$

Combining (5.9) with the weak formulation from the static problem (5.8) one can obtain an alternative definition of the static solution

$$\mathcal{A}(u - u_h, \lambda - \lambda_H; w_h, \delta\lambda_H) = 0 . \tag{5.13}$$

Therefore, we define a mixed elliptic projection $(\tilde{u}_h, \tilde{\lambda}_H)$ for given u and λ as the solution of

$$\mathcal{A}(u - \tilde{u}_h, \lambda - \tilde{\lambda}_H; w_h, \delta\lambda_H) = 0 , \quad \forall w_h \in X_h, \delta\lambda_H \in W_H . \tag{5.14}$$

Then the estimates in this section also hold true for the mixed elliptic projection.

In the estimates, we employ the mesh-dependent norm

$$|||(u_h, \lambda_H)|||_p^2 = \|\nabla u_h\|_{L^2(\Omega)}^2 + \|u_h\|_{1/2,h}^2 + \|\lambda_H\|_{-1/2,h}^2 . \tag{5.15}$$

We define I_h as the Clément interpolation operator projecting functions onto X_h, Π_h as the L^2 projection from $L^2(\Gamma)$ to W_h, and Π_H as the L^2 projection from $L^2(\Gamma)$ to W_H. For $0 < \epsilon < \frac{1}{2}$ we then have the following properties [91, 92]:

Lemma 5.1. *For $u \in H^{3/2-\epsilon}(\Omega)$,*

$$\|u - I_h u\|_{H^1(\Omega)} \leq Ch^{1/2-\epsilon}\|u\|_{H^{3/2-\epsilon}(\Omega)}\,, \tag{5.16}$$

$$\|u - I_h u\|_{L^2(\Gamma)} \leq Ch^{1-\epsilon}\|u\|_{H^{3/2-\epsilon}(\Omega)}\,. \tag{5.17}$$

Lemma 5.2. *For $\lambda \in H^{1/2-\epsilon}(\Gamma)$,*

$$\|\lambda - \Pi_H \lambda\|_{L^2(\Gamma)} \leq CH^{1/2-\epsilon}\|\lambda\|_{H^{1/2-\epsilon}(\Gamma)}\,. \tag{5.18}$$

For $\lambda \in L^2(\Gamma)$,

$$\|\lambda - \Pi_H \lambda\|_{H^{-1/2}(\Gamma)} \leq CH^{1/2}\|\lambda\|_{L^2(\Gamma)}\,, \tag{5.19}$$

$$\|\lambda - \Pi_H \lambda\|_{L^2(\Gamma)} \leq C\|\lambda\|_{L^2(\Gamma)}\,. \tag{5.20}$$

And similar results hold for the projection operator Π_h.

For the duality argument we have proved the following regularity result:

Lemma 5.3. *For any given function ω, consider the elliptic problem*

$$-\nabla \cdot c(\nabla\phi_i) = \omega|_{\Omega_i}, \quad \text{in } \Omega_i\,,\ i \in \{1,2\} \tag{5.21a}$$

$$\phi = 0, \quad \text{on } \partial\Omega, \tag{5.21b}$$

$$\phi = 0, \quad \text{on } \Gamma\,, \tag{5.21c}$$

where $\omega \in L^2(\Omega)$. Set $\theta := -c(\nabla\phi_1)\cdot\mathbf{n}_1 - c(\nabla\phi_2)\cdot\mathbf{n}_2$, then the following inequality holds:

$$\|\phi\|^2_{H^{3/2-\epsilon}(\Omega)} + \|\theta\|^2_{L^2(\Gamma)} \leq C\|\omega\|^2_{L^2(\Omega)}. \tag{5.22}$$

for some constant C.

Proof. For $\phi_i = \phi|_{\Omega_i}$, by [93, Section 5] we get directly

$$\|\phi_i\|_{H^{3/2-\epsilon}(\Omega_i)} \leq C\|\omega_i\|_{L^2(\Omega_i)}, \qquad i = 1,2. \tag{5.23}$$

It remains to estimate the term $\|\theta\|_{L^2(\Gamma)}$. Let $\upsilon \in L^2(\Gamma)$ be an arbitrary function, and let $\tilde{\upsilon} \in H^{1/2}(\Omega_i)$ be a lifting, such that its trace coincides with υ: it is known that the inverse (non tangential) trace operator $\tau^{-1} : L^2(\partial\Omega_i) \to H^{1/2}(\Omega_i)$ is bounded (see for instance [94, Lemma 1.2.6]). Moreover, the gradient operator is bounded from $H^s(\Omega_i) \to H^{s-1}(\partial\Omega_i)$ for all $s > 0$. By integration by parts we have

$$\begin{aligned}
\int_\Gamma \upsilon c(\nabla\phi_i)\cdot\mathbf{n}_i ds &= \int_{\Omega_i} (\tilde{\upsilon}\nabla\cdot c(\nabla\phi_i) + \kappa\nabla\tilde{\upsilon}\cdot\nabla\phi_i)d\mathbf{x} \\
&\leq C(\|\nabla\tilde{\upsilon}\|_{H^{-1/2}(\Omega_i)}\|\nabla\phi\|_{H^{1/2}(\Omega_i)} + \|\tilde{\upsilon}\|_{H^{1/2}(\Omega_i)}\|\Delta\phi\|_{H^{-1/2}(\Omega_i)}) \\
&\leq C\|\tilde{\upsilon}\|_{H^{1/2}(\Omega_i)}(\|\phi\|_{H^{3/2}(\Omega_i)} + \|\Delta\phi\|_{H^{-1/2}(\Omega_i)}) \\
&\leq C\|\upsilon\|_{L^2(\Gamma)}\|\omega\|_{L^2(\Omega_i)}, \qquad i = 1,2,
\end{aligned}$$

and by the arbitrariness of $\upsilon \in L^2(\Gamma)$ we conclude the proof. □

Remark 5.1. We note that the above result is nearly optimal in several ways:

(1) The regularity $\phi_i \in H^{3/2}(\Omega_i)$ and $\Delta\phi_i \in L^2(\Omega_i)$ is optimal (see for instance [93]), in the sense that there exist a Lipschitz domain $\tilde{\Omega}$ and $\tilde{\omega} \in C^\infty(\tilde{\Omega})$, such that the Dirichlet problem

$$\Delta\tilde{\phi} = \tilde{\omega} \in C^\infty(\tilde{\Omega}) \text{ in } \tilde{\Omega}, \quad \tilde{\phi} = 0 \text{ on } \partial\tilde{\Omega}.$$

has a unique solution $\tilde{\phi} \in H^{3/2}(\tilde{\Omega})\backslash\Big(\bigcup_{\epsilon>0} H^{3/2+\epsilon}(\tilde{\Omega})\Big)$, $\Delta\tilde{\phi} \in L^2(\tilde{\Omega})$.
(2) As consequence of the previous counterexample, in general the trace of $\nabla\phi_i$ does not belong to $L^2(\Gamma)$, due to the singularities in its *tangential* part.
(3) We used only the boundedness of the *inverse* trace operator $\tau^{-1} : L^2(\partial\Omega_i) \longrightarrow H^{1/2}(\Omega_i)$. The trace operator $\tau_s : H^s(\Omega_i) \longrightarrow H^{s-1/2}(\partial\Omega_i)$ is bounded for $s \in (1/2, 3/2)$, but not for $s = 1/2$.

Remark 5.2. In the proof we strongly used the fact that the operator $\phi_i \mapsto \nabla\cdot c(\nabla\phi_i) = \kappa\Delta\phi_i$ has constant coefficient κ, thus ϕ_i are solutions to the Laplace equation. Indeed, if ϕ_i were solutions of a more generic divergence type equation, say $\nabla \cdot (A(\mathbf{x})\nabla\phi) = \omega$, with $A(\mathbf{x})$ sufficiently regular (but not constant) such that $\phi \mapsto \nabla \cdot (A(\mathbf{x})\nabla\phi)$ is a strongly elliptic operator, then in general we have only $H^{3/2-\epsilon}(\Omega_i)$ regularity for all $0 < \epsilon < \dfrac{1}{2}$, instead of $H^{3/2}(\Omega_i)$. This could potentially degrade the regularity of θ to $H^{-\epsilon}(\Gamma)$. However, the $H^{3/2-\epsilon}(\Omega)$ regularity of ϕ still holds.

Moreover, to provide the main lemmas for the continuity property and the *inf-sup* condition, we need the following lemmas. Here we assume that $\beta = \dfrac{l}{h} = \mathrm{O}(1/h)$ and the ratio h/H is small enough.

Lemma 5.4. *For any given function $\mu_H \in W_H$, denote by ϕ the solution of the Robin problem for the differential equation*

$$-\nabla \cdot c(\nabla\phi_i) = 0, \quad \text{in } \Omega_i\ ,\ i \in \{1, 2\} \tag{5.24a}$$

$$\phi = 0, \quad \text{on } \partial\Omega, \tag{5.24b}$$

$$c(\nabla\phi_1) \cdot \mathbf{n}_1 + c(\nabla\phi_2) \cdot \mathbf{n}_2 + \beta\phi = \mu_H, \quad \text{on } \Gamma. \tag{5.24c}$$

Then

$$a(\phi, \phi) + \beta\langle\phi, \phi\rangle = \langle\phi, \mu_H\rangle, \tag{5.25}$$

and there exist constants $0 < C_1 < C_2 < \infty$ such that

$$C_1\langle\phi, \mu_H\rangle \le \|\mu_H\|^2_{-1/2,h} \le C_2\langle\phi, \mu_H\rangle. \tag{5.26}$$

Proof. Existence of solution is a direct result from [95]. One can obtain (5.25) by applying the test function ϕ to (5.24a) and integrating. We first want to prove the second inequality

of (5.26). Take $v_h = \Pi_h(\mu_H)$, then we have $\|v_h\|_{L^2(\Gamma)} \le \|\mu_H\|_{L^2(\Gamma)}$. We now show that for h/H sufficiently small, the following statement holds:

$$\|\mu_H\|^2_{L^2(\Gamma)} \le C\langle v_h, \mu_H\rangle \,. \tag{5.27}$$

Since μ_H is piecewise constant, with possible jump discontinuities at element boundaries, we have $\mu_H \in H^{1/2-\epsilon}(\Gamma)$ for any $\epsilon > 0$. Therefore, with the assumption that W_H is strongly regular and when h/H is sufficiently small,

$$\|\mu_H - v_h\|_{L^2(\Gamma)} \le Ch^{1/2-\epsilon}\|\mu_H\|_{H^{1/2-\epsilon}(\Gamma)} \le C\left(\frac{h}{H}\right)^{1/2-\epsilon}\|\mu_H\|_{L^2(\Gamma)} \le \frac{1}{2}\|\mu_H\|_{L^2(\Gamma)} \,. \tag{5.28}$$

Then

$$\|\mu_H\|^2_{L^2(\Gamma)} = \langle v_h, \mu_H\rangle + \langle \mu_H - v_h, \mu_H\rangle = \langle v_h, \mu_H\rangle + \|\mu_H - v_h\|^2_{L^2(\Gamma)} \le \langle v_h, \mu_H\rangle + \frac{1}{4}\|\mu_H\|^2_{L^2(\Gamma)} \,,$$

which implies $\|\mu_H\|^2_{L^2(\Gamma)} \le \frac{4}{3}\langle v_h, \mu_H\rangle$ and gives (5.27).

By an inverse embedding theorem, there exists a linear mapping $\mathcal{M}$ of $H^{1/2}(\Gamma)$ into $H^1(\Omega)$ such that for any function $\theta \in H^{1/2}(\Gamma)$ we have $\mathcal{M}(\theta) = \theta$ on Γ and $\|\mathcal{M}(\theta)\|_{H^1(\Omega)} \le C\|\theta\|_{H^{1/2}(\Gamma)}$. Since $v_h = \Pi_h(\mu_H)$ is continuous, we have $v_h \in H^{1/2}(\Gamma)$ and the strong regularity assumption of W_h yields

$$\|\mathcal{M}(v_h)\|_{H^1(\Omega)} \le C\|v_h\|_{H^{1/2}(\Gamma)} \le C\|v_h\|_{1/2,h} \le C\frac{1}{\sqrt{h}}\|\mu_H\|_{L^2(\Gamma)} \,. \tag{5.29}$$

The above bounds yield

$$\begin{aligned}
\|\mu_H\|^2_{L^2(\Gamma)} &\le C\langle \mu_H, v_h\rangle = C\left(a(\phi, \mathcal{M}(v_h)) + \beta\langle\phi, v_h\rangle\right) \\
&\le C\left(\|\mathcal{M}(v_h)\|_{H^1(\Omega)}\|\phi\|_{H^1(\Omega)} + \beta\|v_h\|_{L^2(\Gamma)}\|\phi\|_{L^2(\Gamma)}\right) \\
&\le C\left(\frac{1}{\sqrt{h}}\|\mu_H\|_{L^2(\Gamma)}\|\phi\|_{H^1(\Omega)} + \frac{1}{\sqrt{h}}\|\mu_H\|_{L^2(\Gamma)}\|\phi\|_{1/2,h}\right) \,,
\end{aligned} \tag{5.30}$$

which, after dividing through by $\|\mu_H\|_{L^2(\Gamma)}/\sqrt{h}$, implies the second inequality of (5.26):

$$\|\mu_H\|_{-1/2,h} \le C\left(\|\phi\|_{H^1(\Omega)} + \|\phi\|_{1/2,h}\right) \le C\sqrt{a(\phi,\phi) + \beta\langle\phi,\phi\rangle} = C\sqrt{\langle\mu_H, \phi\rangle} \,.$$

For the other side of (5.26) we have

$$\langle\phi, \mu_H\rangle \le \|\phi\|_{1/2,h}\|\mu_H\|_{-1/2,h} \le C\sqrt{a(\phi,\phi) + \beta\langle\phi,\phi\rangle}\|\mu_H\|_{-1/2,h} = C\sqrt{\langle\phi,\mu_H\rangle}\|\mu_H\|_{-1/2,h} \,,$$

and thus $\langle\phi, \mu_H\rangle \le C\|\mu_H\|^2_{-1/2,h}$. We have finished the proof. □

Lemma 5.5. *Assuming that Ω has finite diameter, then for any given function $\mu_H \in W_H$, denote by ϕ the solution of the Robin problem in* (5.24)*, we have $\phi \in H^{3/2-\epsilon}(\Omega)$ for all $\epsilon > 0$. Moreover, for $1 \le s \le 3/2 - \epsilon$, the following inequality holds*

$$\|\phi\|_{H^s(\Omega)} \le C\sqrt{h}\|\mu_H\|_{H^{s-1}(\Gamma)}. \tag{5.31}$$

Proof. For $s = 1$, Lemma 5.4 gives

$$\|\phi\|^2_{H^1(\Omega)} \le Ca(\phi,\phi) \le C\langle\phi,\mu_H\rangle \le Ch\|\mu_H\|^2_{L^2(\Gamma)}. \tag{5.32}$$

For the case $1 < s = 3/2 - \epsilon$, we separate the proof for 2D and 3D cases. Since μ_H is piecewise constant, $\mu_H \in H^{1/2-\epsilon}(\Gamma)$ for any ϵ>0. Note that for any piecewise constant μ_H, we can approximate it with a sequence of smooth functions which are obtained by modifying μ_H on arbitrarily small sets near the jump points. Therefore, we first prove the estimate for $\mu_H \in H^{1-\epsilon}(\Gamma)$. Later we will extend the proof to $\mu_H \in H^{1/2-\epsilon}(\Gamma)$ for all $\epsilon > 0$. For the 2D case, the Gagliardo semi-norm can be written as

$$[\nabla\phi]^2_{H^{1/2-\epsilon}(\Omega)} := \int_{\Omega\times\Omega} \frac{|\nabla\phi(\mathbf{x}) - \nabla\phi(\mathbf{y})|^2}{|x-y|^{3-2\epsilon}} d\mathbf{x}d\mathbf{y} = \sum_{j=1}^{2} \int_{\Omega_j\times\Omega_j} \frac{|\nabla\phi(\mathbf{x}) - \nabla\phi(\mathbf{y})|^2}{|\mathbf{x}-\mathbf{y}|^{3-2\epsilon}} d\mathbf{x}d\mathbf{y}$$
$$+ \int_{\Omega_1\times\Omega_2} \frac{|\nabla\phi(\mathbf{x}) - \nabla\phi(\mathbf{y})|^2}{|\mathbf{x}-\mathbf{y}|^{3-2\epsilon}} d\mathbf{x}d\mathbf{y} + \int_{\Omega_2\times\Omega_1} \frac{|\nabla\phi(\mathbf{x}) - \nabla\phi(\mathbf{y})|^2}{|\mathbf{x}-\mathbf{y}|^{3-2\epsilon}} d\mathbf{x}d\mathbf{y}.$$

To prove $\|\phi\|^2_{H^{3/2-\epsilon}(\Omega)} < Ch\|\mu_H\|^2_{H^{1/2-\epsilon}(\Gamma)}$ it suffices to show

$$\int_{\Omega_1\times\Omega_1} \frac{|\nabla\phi(\mathbf{x}) - \nabla\phi(\mathbf{y})|^2}{|\mathbf{x}-\mathbf{y}|^{3-2\epsilon}} d\mathbf{x}d\mathbf{y} = \|\phi\|^2_{H^{3/2-\epsilon}(\Omega_1)} \le Ch\|\mu_H\|^2_{H^{1/2-\epsilon}(\Gamma)} \tag{5.33}$$

$$\int_{\Omega_1\times\Omega_2} \frac{|\nabla\phi(\mathbf{x}) - \nabla\phi(\mathbf{y})|^2}{|\mathbf{x}-\mathbf{y}|^{3-2\epsilon}} d\mathbf{x}d\mathbf{y} \le Ch\|\mu_H\|^2_{H^{1/2-\epsilon}(\Gamma)}, \tag{5.34}$$

as the proof for the other two integral terms is completely analogous. To prove (5.33), we rewrite the problem as

$$\begin{aligned} -\nabla\cdot c(\nabla\phi_i) &= 0, \quad \text{in } \Omega_i\ ,\ i \in \{1,2\} \\ \phi &= 0, \quad \text{on } \partial\Omega, \\ \phi &= \frac{1}{\beta}(\mu_H + \theta) \quad \text{on } \Gamma, \end{aligned} \tag{5.35}$$

where $\theta := -c(\nabla\phi_1)\cdot\mathbf{n}_1 - c(\nabla\phi_2)\cdot\mathbf{n}_2$ is the normal jump of the gradient across Γ. In the following we will prove the estimate for $\|\theta\|_{L^2(\Gamma)}$ as

$$\|\theta\|_{L^2(\Gamma)} \le \|\mu_H\|_{L^2(\Gamma)}. \tag{5.36}$$

By integration by parts we have

$$\int_\Gamma \phi_1 c(\nabla\phi_1)\cdot\mathbf{n}_1 ds = \int_{\Omega_1} [\phi_1\nabla\cdot c(\nabla\phi_1) + \kappa|\nabla\phi_1|^2] d\mathbf{x} = \kappa\|\nabla\phi_1\|^2_{L^2(\Omega_1)},$$
$$\int_\Gamma \phi_2 c(\nabla\phi_2)\cdot\mathbf{n}_2 ds = \int_{\Omega_2} [\phi_2\nabla\cdot c(\nabla\phi_2) + \kappa|\nabla\phi_2|^2] d\mathbf{x} = \kappa\|\nabla\phi_2\|^2_{L^2(\Omega_2)},$$

hence

$$\begin{aligned} \kappa\|\nabla\phi\|^2_{L^2(\Omega)} &= \int_\Gamma \phi(c(\nabla\phi_1)\cdot\mathbf{n}_1 + c(\nabla\phi_2)\cdot\mathbf{n}_2) ds \\ &= \int_\Gamma \frac{1}{\beta}(\mu_H - (c(\nabla\phi_1)\cdot\mathbf{n}_1 + c(\nabla\phi_2)\cdot\mathbf{n}_2))(c(\nabla\phi_1)\cdot\mathbf{n}_1 + c(\nabla\phi_2)\cdot\mathbf{n}_2) ds \\ &= \frac{h}{l}\int_\Gamma [\mu_H(c(\nabla\phi_1)\cdot\mathbf{n}_1 + c(\nabla\phi_2)\cdot\mathbf{n}_2) - |c(\nabla\phi_1)\cdot\mathbf{n}_1 + c(\nabla\phi_2)\cdot\mathbf{n}_2|^2] ds, \end{aligned}$$

which then gives

$$\begin{aligned}\| - c(\nabla\phi_1)\cdot\mathbf{n}_1 - c(\nabla\phi_2)\cdot\mathbf{n}_2\|^2_{L^2(\Gamma)} &\le \int_\Gamma \mu_H(c(\nabla\phi_1)\cdot\mathbf{n}_1 + c(\nabla\phi_2)\cdot\mathbf{n}_2)ds\\ &\le \|\mu_H\|_{L^2(\Gamma)}\| - c(\nabla\phi_1)\cdot\mathbf{n}_1 - c(\nabla\phi_2)\cdot\mathbf{n}_2\|_{L^2(\Gamma)},\end{aligned}$$

which proves (5.36). This implies $\theta \in H^{-1/2}(\Gamma)$, and by the trace theorem we have

$$\|\theta\|_{H^{-1/2}(\Gamma)} \le C\|\phi\|_{H^1(\Omega)} \le Ch^{1/2}\|\mu_H\|_{L^2(\Gamma)}.$$

Since $\mu_H \in H^{1/2}(\Gamma)$, we have also

$$\begin{aligned}\kappa\|\nabla\phi\|^2_{L^2(\Omega)} = \frac{h}{l}\int_\Gamma[-\mu_H\theta - |\theta|^2]ds &\le \frac{h}{l}\|\mu_H\|_{H^{1/2}(\Gamma)}\|\theta\|_{H^{-1/2}(\Gamma)} - \frac{h}{l}\|\theta\|^2_{L^2(\Gamma)}\\ &\le Ch\|\mu_H\|_{H^{1/2}(\Gamma)}\|\phi\|_{H^1(\Omega)} - \frac{h}{l}\|\theta\|^2_{L^2(\Gamma)}\\ &\le Ch^{3/2}\|\mu_H\|_{H^{1/2}(\Gamma)}\|\mu_H\|_{L^2(\Gamma)} - \frac{h}{l}\|\theta\|^2_{L^2(\Gamma)},\end{aligned}$$

hence

$$\begin{aligned}\|\phi\|_{H^1(\Omega)} &\le Ch\|\mu_H\|_{H^{1/2}(\Gamma)},\\ \|\theta\|^2_{L^2(\Gamma)} &\le Ch^{1/2}\|\mu_H\|_{H^{1/2}(\Gamma)}\|\mu_H\|_{L^2(\Gamma)},\\ \|h(\mu_H+\theta)\|_{H^{1/2}(\Gamma)} = l\|\phi\|_{H^{1/2}(\Gamma)} &\le C\|\phi\|_{H^1(\Omega)} \le Ch\|\mu_H\|_{H^{1/2}(\Gamma)}\\ &\Longrightarrow \|\mu_H+\theta\|_{H^{1/2}(\Gamma)} \le C\|\mu_H\|_{H^{1/2}(\Gamma)}\\ &\Longrightarrow \|\theta\|_{H^{1/2}(\Gamma)} \le \|\mu_H+\theta\|_{H^{1/2}(\Gamma)} + \|\mu_H\|_{H^{1/2}(\Gamma)} \le C\|\mu_H\|_{H^{1/2}(\Gamma)}.\end{aligned}$$

The last estimate is crucial: we can then approximate θ with functions $\theta_n \in H^{1-\epsilon}(\Gamma)$ such that

$$\theta_n \to \theta \text{ strongly in } H^{1/2}(\Gamma), \qquad \|\theta_n\|_{H^{1-\epsilon}(\Gamma)} \le h^{\epsilon-1/2}\|\theta_n\|_{H^{1/2}(\Gamma)},$$

and consider the Dirichlet problems

$$\begin{aligned}-\nabla\cdot c(\nabla\phi_{ni}) &= 0, \quad \text{in } \Omega_i\,,\ i\in\{1,2\}\\ \phi_n &= 0, \quad \text{on } \partial\Omega,\\ \phi_n &= \frac{1}{\beta}(\mu_H+\theta_n) \quad \text{on } \Gamma,\end{aligned}$$

Since $\theta_n \to \theta$ strongly in $H^{1/2}(\Gamma)$, it is straightforward to check that ϕ_{ni} weakly converge to ϕ_i in $H^{3/2-\epsilon}(\Omega_i)$ where $i = 1$ or 2. Thus by [93, Section 5] we infer

$$\begin{aligned}\|\phi_i\|_{H^{3/2-\epsilon}(\Omega_i)} &\le \liminf_{n\to+\infty}\|\phi_{ni}\|_{H^{3/2-\epsilon}(\Omega_i)}\\ &\le Ch\liminf_{n\to+\infty}(\|\mu_H\|_{H^{1-\epsilon}(\Gamma)} + \|\theta_n\|_{H^{1-\epsilon}(\Gamma)})\\ &\le Ch^{1/2+\epsilon}\liminf_{n\to+\infty}(\|\mu_H\|_{H^{1/2}(\Gamma)} + \|\theta_n\|_{H^{1/2}(\Gamma)})\\ &= Ch^{1/2+\epsilon}(\|\mu_H\|_{H^{1/2}(\Gamma)} + \|\theta\|_{H^{1/2}(\Gamma)})\\ &\le Ch^{1/2+\epsilon}\|\mu_H\|_{H^{1/2}(\Gamma)} \le Ch^{1/2}\|\mu_H\|_{H^{1/2-\epsilon}(\Gamma)}. \qquad (5.37)\end{aligned}$$

which concludes the proof of (5.33).

As with u in the proof of Theorem 4.2, the function ϕ is obtained by "gluing" together ϕ_i. So $\phi|_{\Omega_i} = \phi_i$, and we can check that $\phi \in H^{3/2-\epsilon}(\Omega)$ by showing that the Gagliardo seminorm $[\nabla\phi]_{1/2-\epsilon}$ is finite. Let $\widetilde{\nabla\phi_i} \in H^{3/2-\epsilon}(\Omega)$ be the extensions to zero of $\nabla\phi_i$ outside Ω_i, similar as in (4.6) we can show that for any test function $\varphi \in C_0^\infty(\Omega)$ we have

$$\int_\Omega (\widetilde{\nabla\phi_1} + \widetilde{\nabla\phi_2}) \cdot \varphi d\mathbf{x} = \int_\Omega \nabla\phi \cdot \varphi d\mathbf{x}.$$

Thus $\nabla\phi = \widetilde{\nabla\phi_1} + \widetilde{\nabla\phi_2} \in H^{1/2-\epsilon}(\Omega)$ and $\phi \in H^{3/2-\epsilon}(\Omega)$. Therefore,

$$\|\phi\|_{H^{3/2-\epsilon}(\Omega)} \le C \sum_{i=1}^{2} \|\phi_i\|_{H^{3/2-\epsilon}(\Omega_i)} \le Ch^{1/2} \|\mu_H\|_{H^{1/2-\epsilon}(\Gamma)}. \tag{5.38}$$

Thus we have concluded the proof for $\mu_H \in H^{1-\epsilon}(\Gamma)$. For generic $\mu_H \in H^{1/2-\epsilon}(\Gamma)$, we can approximate μ_H with a sequence of smoother functions $\mu_H^{(n)} \subseteq H^{1-\epsilon}(\Gamma)$ such that $\mu_H^{(n)} \to \mu_H$ in $H^{1/2-\epsilon}(\Gamma)$. Repeating the above arguments for $\mu_H^{(n)}$, denoting by $\phi^{(n)}$ the solution of

$$-\nabla \cdot c(\nabla\phi_i^{(n)}) = 0, \quad \text{in } \Omega_i\ ,\ i \in \{1,2\}, \tag{5.39}$$

$$\phi_1^{(n)} = \phi_2^{(n)} = 0, \quad \text{on } \partial\Omega, \tag{5.40}$$

$$\phi_1^{(n)} = \phi_2^{(n)} = \phi^{(n)}, \quad \text{on } \Gamma, \tag{5.41}$$

$$c(\nabla\phi_1^{(n)}) \cdot \mathbf{n}_1 + c(\nabla\phi_2^{(n)}) \cdot \mathbf{n}_2 + \beta\phi^{(n)} = \mu_H^{(n)}, \quad \text{on } \Gamma, \tag{5.42}$$

the inequality (5.38) gives

$$\|\phi^{(n)}\|_{H^{3/2-\epsilon}(\Omega)} \le C' h^{1/2} \|\mu_H^{(n)}\|_{H^{1/2-\epsilon}(\Gamma)},$$

where the right-hand side quantities is uniformly bounded from above as $n \to +\infty$. Thus the sequence $\phi^{(n)}$ is uniformly bounded in $H^{3/2-\epsilon}(\Omega)$, hence upon extracting a subsequence (which we do not relabel) $\phi^{(n)} \to \phi$ in $H^{3/2-\epsilon}(\Omega)$, with ϕ being the solution of (5.24). Thus by the lower-semicontinuity of the norm $\|\cdot\|_{H^{3/2-\epsilon}(\Omega)}$ we infer

$$\|\phi\|_{H^{3/2-\epsilon}(\Omega)} \le \liminf_{n\to+\infty} C' h^{1/2} \|\mu_H^{(n)}\|_{H^{1/2-\epsilon}(\Gamma)} = C' h^{1/2} \|\mu_H\|_{H^{1/2-\epsilon}(\Gamma)},$$

concluding the proof for 2D case. The 3D case can be similarly proved with the above procedure, except that the Gagliardo semi-norm should be modified as

$$[\nabla\phi]^2_{H^{1/2-\epsilon}(\Omega)} := \int_{\Omega\times\Omega} \frac{|\nabla\phi(\mathbf{x}) - \nabla\phi(\mathbf{y})|^2}{|\mathbf{x}-\mathbf{y}|^{4-2\epsilon}} d\mathbf{x}d\mathbf{y}.$$

and we have then finished the proof. □

We now prove the continuity property and the *inf-sup* condition of $\mathcal{A}(\cdot,\cdot;\cdot,\cdot)$ as follows:

Lemma 5.6. *For all* $(v,\mu) \in H_0^1(\Omega)\times L^2(\Gamma)$, $(w_h, \delta\lambda_H) \in X_h \times W_H$, $\mathcal{A}(v,\mu;w_h,\delta\lambda_H)$ *satisfies the continuous property:*

$$\mathcal{A}(v,\mu;w_h,\delta\lambda_H) \le C|||(v,\mu)|||_p |||(w_h,\delta\lambda_H)|||_p. \tag{5.43}$$

Proof. From the definition of $\mathcal{A}$ and the Schwarz' inequality one can establish Lemma 5.6. □

Lemma 5.7. *Let $(v_h, \mu_H) \in X_h \times W_H$. When h/H is small enough, the following inf-sup property holds:*

$$\sup_{|||(w_h,\delta\lambda_H)|||_p=1} \mathcal{A}(v_h, \mu_H; w_h, \delta\lambda_H) \geq C|||(v_h, \mu_H)|||_p \,. \tag{5.44}$$

Proof. For a given μ_H, denote by ϕ the solution of the Robin problem in (5.24), then

$$a(v_h, \phi) = \langle v_h, \mu_H\rangle - \beta \langle v_h, \phi\rangle \,, \tag{5.45}$$

and from Lemma 5.4, the following bound holds for ϕ:

$$\|\mu_H\|^2_{-1/2,h} \leq C\langle \mu_H, P(\phi)\rangle \,. \tag{5.46}$$

With the above two properties one can then obtain the bound for $\mathcal{A}(v_h, \mu_H; u_h + \phi, 2\mu_H)$:

$$\begin{aligned}\mathcal{A}(v_h, \mu_H; v_h + \phi, 2\mu_H) =& a(v_h, v_h) + \langle \mu_H, P(\phi)\rangle + \beta \langle v_h, v_h\rangle \\ \geq& \kappa\|\nabla v_h\|^2_{L^2(\Omega)} + C^*\|\mu_H\|^2_{-1/2,h} + l\|v_h\|^2_{1/2,h} \,.\end{aligned} \tag{5.47}$$

where the constant C^* is associated with the inequality (5.46). Taking $\phi_h = I_h(\phi)$, the following estimates hold

$$\|\phi_h - \phi\|_{H^1(\Omega)} \leq Ch^{1/2-\epsilon}\|\phi\|_{H^{3/2-\epsilon}(\Omega)} \leq h^{1-\epsilon}\|\mu_H\|_{H^{1/2-\epsilon}(\Gamma)} \leq C\left(\frac{h}{H}\right)^{1/2-\epsilon} \|\mu_H\|_{-1/2,h}, \tag{5.48}$$

$$\|\phi_h - \phi\|_{L^2(\Gamma)} \leq Ch^{1-\epsilon}\|\phi\|_{H^{3/2-\epsilon}(\Omega)} \leq C\sqrt{h}\left(\frac{h}{H}\right)^{1/2-\epsilon} \|\mu_H\|_{-1/2,h}. \tag{5.49}$$

Taking $w_h = v_h + \phi_h$ and $\delta\lambda_H = 2\mu_H$, we have

$$\begin{aligned}\mathcal{A}(v_h, \mu_H; w_h, \delta\lambda_H) \geq& \kappa\|\nabla v_h\|^2_{L^2(\Omega)} + C^*\|\mu_H\|^2_{-1/2,h} + l\|v_h\|^2_{1/2,h} + a(v_h, \phi_h - \phi) \\ &+ \langle \mu_H, P(\phi_h - \phi)\rangle + \beta \langle v_h, \phi_h - \phi\rangle \,.\end{aligned} \tag{5.50}$$

We then bound the last three terms on the right hand side, namely:

$$a(v_h, \phi_h - \phi) \geq -\frac{\kappa}{2}\|\nabla v_h\|_{L^2(\Omega)} - C\|\nabla(\phi_h - \phi)\|^2_{L^2(\Omega)} \geq -\frac{\kappa}{2}\|\nabla v_h\|_{L^2(\Omega)} - C\left(\frac{h}{H}\right)^{1-2\epsilon} \|\mu_H\|^2_{-1/2,h},$$

$$\langle \mu_H, P(\phi_h - \phi)\rangle \geq -\frac{1}{2}C^*\|\mu_H\|^2_{-1/2,h} - C\|\phi_h - \phi\|^2_{1/2,h} \geq -\frac{1}{2}C^*\|\mu_H\|^2_{-1/2,h} - C\left(\frac{h}{H}\right)^{1-2\epsilon} \|\mu_H\|^2_{-1/2,h},$$

$$\beta \langle v_h, \phi_h - \phi\rangle \geq -\frac{l}{2h}\|v_h\|^2_{L^2(\Gamma)} - \frac{C}{h}\|\phi_h - \phi\|^2_{L^2(\Gamma)} \geq -\frac{l}{2}\|v_h\|^2_{1/2,h} - C\left(\frac{h}{H}\right)^{1-2\epsilon} \|\mu_H\|^2_{-1/2,h} \,.$$

Substituting the above three estimates into (5.50) yields

$$\begin{aligned}\mathcal{A}(v_h, \mu_H; u_h + \phi_h, 2\mu_H) \geq& \frac{\kappa}{2}\|\nabla v_h\|^2_{L^2(\Omega)} + \frac{C^*}{2}\|\mu_H\|^2_{-1/2,h} + \frac{l}{2}\|v_h\|^2_{1/2,h} - C\left(\frac{h}{H}\right)^{1-2\epsilon} \|\mu_H\|^2_{-1/2,h} \\ =& C\left(\|\nabla v_h\|^2_{L^2(\Omega)} + \left(C^* - C_1\left(\frac{h}{H}\right)^{1-2\epsilon}\right)\|\mu_H\|^2_{-1/2,h} + \|v_h\|^2_{1/2,h}\right) \,.\end{aligned}$$

On the other hand, with Lemma 5.4, (5.48)-(5.49) and the facts

$$\|\phi\|_{1/2,h}^2 = \frac{1}{l}(-a(\phi,\phi) + \langle\phi,\mu_H\rangle) \le C\,\langle\phi,\mu_H\rangle \le C\|\mu_H\|_{-1/2,h}^2,$$

we have the following estimate

$$\begin{aligned}
&\|\nabla w_h\|_{L^2(\Omega)}^2 + \|\delta\lambda_H\|_{-1/2,h}^2 + \|w_h\|_{1/2,h}^2 = \|\nabla v_h + \nabla\phi_h\|_{L^2(\Omega)}^2 + \|2\mu_H\|_{-1/2,h}^2 + \|v_h+\phi_h\|_{1/2,h}^2\\
\le& C\left(\|\nabla v_h\|_{L^2(\Omega)}^2 + \|\nabla\phi\|_{L^2(\Omega)}^2 + \|\nabla(\phi-\phi_h)\|_{L^2(\Omega)}^2 + \|\mu_H\|_{-1/2,h}^2 + \|v_h\|_{1/2,h}^2\right.\\
&\left.+\|\phi-\phi_h\|_{1/2,h}^2 + \|\phi\|_{1/2,h}^2\right)\\
\le& C\left(\|\nabla v_h\|_{L^2(\Omega)}^2 + \|\mu_H\|_{-1/2,h}^2 + \|v_h\|_{1/2,h}^2\right).
\end{aligned}$$

Therefore, we have $\mathcal{A}(v_h,\mu_H;w_h,\delta\lambda_H) \ge C|||(v_h,\mu_H)|||_p|||(w_h,\delta\lambda_H)|||_p$ which finishes the proof. □

Lemma 5.8. *When h/H is small enough, there exists a constant C such that for any given function $\mu_H \in W_H$, the following inf-sup condition holds true:*

$$\sup_{w_h\in X_h}\frac{\langle w_h,\mu_H\rangle}{\|w_h\|_{H^1(\Omega)} + \|w_h\|_{1/2,h}} \ge C\|\mu_H\|_{-1/2,h}\,. \tag{5.51}$$

Proof. Set $v_h = 0$ in (5.44). The supremum is clearly attained for $\delta\lambda_H = 0$, producing (5.51). □

With the above lemmas, we can prove the error estimates in the following theorem

Theorem 5.1. *Let $(u,\lambda) \in H^{3/2-\epsilon}(\Omega)\times L^2(\Gamma)$ be the solution of* (5.8) *and $(\tilde{u}_h,\tilde{\lambda}_H) \in X_h\times W_H$ be the solutions of* (5.9)*. Then for $\beta = \dfrac{l}{h}$, when h/H is small, the following estimates hold true:*

$$|||(u-\tilde{u}_h,\lambda-\tilde{\lambda}_H)|||_p \le Ch^{1-2\epsilon}\left(\|u\|_{H^{3/2-\epsilon}(\Omega)} + \|\lambda\|_{L^2(\Gamma)}\right), \tag{5.52}$$

$$\|u-\tilde{u}_h\|_{L^2(\Omega)} \le Ch^{1/2-\epsilon}H^{1/2}\left(\|u\|_{H^{3/2-\epsilon}(\Omega)} + \|\lambda\|_{L^2(\Gamma)}\right). \tag{5.53}$$

Proof. From the triangle inequality we can obtain

$$|||(u-\tilde{u}_h,\lambda-\tilde{\lambda}_H)|||_p \le |||(u-I_hu,\lambda-\Pi_H\lambda)|||_p + |||(I_hu-\tilde{u}_h,\Pi_H\lambda-\tilde{\lambda}_H)|||_p\,. \tag{5.54}$$

For the first term, given $h \ll 1$, we have

$$\begin{aligned}
|||(u-I_hu,\lambda-\Pi_H\lambda)|||_p^2 &= \|\nabla(u-I_hu)\|_{L^2(\Omega)}^2 + \|\lambda-\Pi_H\lambda\|_{-1/2,h}^2 + \|u-I_hu\|_{1/2,h}^2\\
&\le Ch^{1-2\epsilon}\|u\|_{H^{3/2-\epsilon}(\Omega)}^2 + Ch\|\lambda\|_{L^2(\Gamma)}^2\,.
\end{aligned}$$

For the second term, the proof of Lemma 5.7 shows that there exists $(w_h,\delta\lambda_H) \in X_h\times W_H$ such that $|||(w_h,\delta\lambda_H)|||_p = 1$ and

$$\begin{aligned}
|||(I_hu-\tilde{u}_h,\Pi_H\lambda-\tilde{\lambda}_H)|||_p &\le C\mathcal{A}(I_hu-\tilde{u}_h,\Pi_H\lambda-\tilde{\lambda}_H;w_h,\delta\lambda_H)\\
&= C\left(\mathcal{A}(u-\tilde{u}_h,\lambda-\tilde{\lambda}_H;w_h,\delta\lambda_H) + \mathcal{A}(I_hu-u,\Pi_H\lambda-\lambda;w_h,\delta\lambda_H)\right).
\end{aligned} \tag{5.55}$$

From the alternative definition given in (5.14), the first term of (5.55) should be equal to 0. The estimate for the second part of (5.55) can be derived from Lemma 5.6:

$$\mathcal{A}(I_h u - u, \Pi_H \lambda - \lambda; w_h, \delta\lambda_H) \le C|||u - I_h u, \lambda - \Pi_H \lambda|||_p \le Ch^{1/2-\epsilon}\|u\|^2_{H^{3/2-\epsilon}(\Omega)} + Ch^{1/2}\|\lambda\|^2_{L^2(\Gamma)} .$$

The estimate (5.52) can then be obtained

$$|||(I_h u - \tilde{u}_h, \Pi_H \lambda - \tilde{\lambda}_H)|||_p \le Ch^{1-2\epsilon}\left(\|u\|_{H^{3/2-\epsilon}(\Omega)} + \|\lambda\|_{L^2(\Gamma)}\right) ,$$

To estimate the L^2 error, we apply an Aubin–Nitsche duality argument by introducing the Dirichlet problem of finding ϕ satisfying

$$-\nabla \cdot c(\nabla\phi_i) = u - \tilde{u}_h, \quad \text{in } \Omega_i \ , \ i \in \{1, 2\}, \tag{5.56a}$$

$$\phi = 0, \quad \text{on } \partial\Omega, \tag{5.56b}$$

$$\phi = 0, \quad \text{on } \Gamma. \tag{5.56c}$$

Setting $\theta = -c(\nabla\phi_1) \cdot \mathbf{n}_1 - c(\nabla\phi_2) \cdot \mathbf{n}_2$, from Lemma 5.3 the following bound holds for ϕ and θ

$$\|\phi\|^2_{H^{3/2-\epsilon}(\Omega)} + \|\theta\|^2_{L^2(\Gamma)} \le C \|u - \tilde{u}_h\|^2_{L^2(\Omega)} . \tag{5.57}$$

Taking an inner product of (5.56a) and $u - \tilde{u}_h$ gives

$$\|u - \tilde{u}_h\|^2_{L^2(\Omega)} = a(\phi - I_h\phi, u - \tilde{u}_h) + a(I_h\phi, u - \tilde{u}_h) + \langle\theta, u - \tilde{u}_h\rangle \ . \tag{5.58}$$

With Lemma 5.3 we can provide the bound for each of the above three terms. Firstly,

$$\begin{aligned} a\left(\phi - I_h\phi, u - \tilde{u}_h\right) &\le Ch^{1-2\epsilon}\|\phi\|_{H^{3/2-\epsilon}(\Omega)}\left(\|u\|_{H^{3/2-\epsilon}(\Omega)} + \|\lambda\|_{L^2(\Gamma)}\right) \\ &\le Ch^{1-2\epsilon}\|u - \tilde{u}_h\|_{L^2(\Omega)}\left(\|u\|_{H^{3/2-\epsilon}(\Omega)} + \|\lambda\|_{L^2(\Gamma)}\right) . \end{aligned} \tag{5.59}$$

Secondly, from (5.14) and the fact that $\phi = 0$ on Γ

$$\begin{aligned} a(I_h\phi, u - \tilde{u}_h) &= \left\langle \lambda - \tilde{\lambda}_H, \phi - I_h\phi \right\rangle + \beta\langle\phi - I_h\phi, u - \tilde{u}_h\rangle \\ &\le Ch^{1-2\epsilon}\|u - \tilde{u}_h\|_{L^2(\Omega)}\left(\|u\|_{H^{3/2-\epsilon}(\Omega)} + \|\lambda\|_{L^2(\Gamma)}\right) . \end{aligned} \tag{5.60}$$

For the last term in (5.58), from the fact that $\langle\Pi_H\theta, u - \tilde{u}_h\rangle = 0$, we divide it into two parts:

$$\begin{aligned} \langle\theta, u - \tilde{u}_h\rangle = \langle\theta - \Pi_H\theta, u - \tilde{u}_h\rangle &\le CH^{1/2}h^{1/2-\epsilon}\|\theta\|_{L^2(\Gamma)}\left(\|u\|_{H^{3/2-\epsilon}(\Omega)} + \|\lambda\|_{L^2(\Gamma)}\right) \\ &\le CH^{1/2}h^{1/2-\epsilon}\|u - \tilde{u}_h\|_{L^2(\Omega)}\left(\|u\|_{H^{3/2-\epsilon}(\Omega)} + \|\lambda\|_{L^2(\Gamma)}\right) . \end{aligned} \tag{5.61}$$

Combining (5.58)–(5.61), and given the fact that $h < H$, one can get

$$\|u - \tilde{u}_h\|_{L^2(\Omega)} \le Ch^{1/2-\epsilon}H^{1/2}\left(\|u\|_{H^{3/2-\epsilon}(\Omega)} + \|\lambda\|_{L^2(\Gamma)}\right) .$$

We have then finished the error estimate of the projection-based DAL method on the static problem. □

Remark 5.3. The analysis for linear finite elements can be extended to higher-order elements, but the convergence rate would not improve. Nevertheless, in practice, higher-order approximations of fluid mechanics may be beneficial for representing complex flow features away from the boundary; cf. the reasoning in [96, Section 3].

5.2. *Fully discrete: Parabolic interface problem*

By taking a (weak) time derivative of (5.14), it can be seen that in the projection-based DAL problem the mixed elliptic projection (5.10) commutes with the time derivative. Based on the analysis for the static problem in Section 5.1, we will have the following lemma for the projection-based DAL method:

Lemma 5.9. *For given u and λ, we have the following estimates for their mixed elliptic projection $(\tilde{u}_h, \tilde{\lambda}_H)$ defined in* (5.14)*:*

$$|||(u - \tilde{u}_h, \lambda - \tilde{\lambda}_H)|||_p^2 \leq Ch^{1-2\epsilon} \left(\|u\|_{H^{3/2-\epsilon}(\Omega)}^2 + \|\lambda\|_{L^2(\Gamma)}^2 \right) , \tag{5.62}$$

$$\|u - \tilde{u}_h\|_{L^2(\Omega)}^2 \leq Ch^{1-2\epsilon} H \left(\|u\|_{H^{3/2-\epsilon}(\Omega)}^2 + \|\lambda\|_{L^2(\Gamma)}^2 \right) , \tag{5.63}$$

$$\left| \left| \left| \left(\frac{\partial u}{\partial t} - \frac{\partial \tilde{u}_h}{\partial t}, \frac{\partial \lambda}{\partial t} - \frac{\partial \tilde{\lambda}_H}{\partial t} \right) \right| \right|_p^2 \leq Ch^{1-2\epsilon} \left(\left\| \frac{\partial u}{\partial t} \right\|_{H^{3/2-\epsilon}(\Omega)}^2 + \left\| \frac{\partial \lambda}{\partial t} \right\|_{L^2(\Gamma)}^2 \right) , \tag{5.64}$$

$$\left\| \frac{\partial u}{\partial t} - \frac{\partial \tilde{u}_h}{\partial t} \right\|_{L^2(\Omega)}^2 \leq Ch^{1-2\epsilon} H \left(\left\| \frac{\partial u}{\partial t} \right\|_{H^{3/2-\epsilon}(\Omega)}^2 + \left\| \frac{\partial \lambda}{\partial t} \right\|_{L^2(\Gamma)}^2 \right) . \tag{5.65}$$

Here by $\dfrac{\partial}{\partial t}$ we denote the weak time derivative as defined in [97, Section 5.9.2] and the estimates for the derivatives hold true for a.e. $t \in (0, T)$.

Let Δt be the time step size and $T = N\Delta t$. We employ the backward Euler method for time integration, and obtain the following fully discrete scheme for the projection-based DAL method at the $(n+1)$-th time step. Denoting $\overline{\partial}_t v^{n+1} = \dfrac{v^{n+1} - v^n}{\Delta t}$, given (u_h^n, λ_H^n) find $(u_h^{n+1}, \lambda_H^{n+1}) \in X_h \times W_H$ such that

$$\begin{aligned} &\left(\overline{\partial}_t u_h^{n+1}, w_h \right) - \Delta t \left\langle \overline{\partial}_t \lambda_H^{n+1}, w_h \right\rangle + a(u_h^{n+1}, w_h) + \left\langle \lambda_H^{n+1}, w_h \right\rangle + \beta \left\langle u_h^{n+1}, w_h \right\rangle \\ &= \left(f(t^{n+1}), w_h \right) + \beta \left\langle g(t^{n+1}), w_h \right\rangle , \quad \forall w_h \in X_h , \end{aligned} \tag{5.66a}$$

$$\Delta t \left\langle \overline{\partial}_t \lambda_H^{n+1}, \delta\lambda_H \right\rangle = \beta \left\langle u_h^{n+1} - g(t^{n+1}), \delta\lambda_H \right\rangle , \quad \forall \delta\lambda_H \in W_H , \tag{5.66b}$$

$$u_h^0 = I_h u_0 , \tag{5.66c}$$

$$\lambda_H^0 = 0 . \tag{5.66d}$$

The above fully-discrete method can be written in an equivalent form: Find $(u_h^{n+1}, \lambda_H^{n+1}) \in X_h \times W_H$ such that $\forall w_h \in X_h, \delta\lambda_H \in W_H$,

$$\left(\overline{\partial}_t u_h^{n+1}, w_h \right) - \Delta t \left\langle \overline{\partial}_t \lambda_H^{n+1}, w_h \right\rangle + \frac{\Delta t}{\beta} \left\langle \overline{\partial}_t \lambda_H^{n+1}, \delta\lambda_H \right\rangle + \mathcal{A}(u_h^{n+1}, \lambda_H^{n+1}; w_h, \delta\lambda_H) = \mathcal{F}(w_h, \delta\lambda_H). \tag{5.67}$$

We can then prove the following theorem:

Theorem 5.2. *Let $(u, \lambda) \in H^2(0, T; H^{3/2-\epsilon}(\Omega)) \times H^1(0, T; L^2(\Gamma))$ be the solution of* (4.2) *and $(u_h^{n+1}, \lambda_H^{n+1}) \in X_h \times W_H$ be the solutions of* (5.66)*, then when the element ratio h/H*

is small enough and $\beta = \dfrac{l}{h}$*, the following error estimates for the projection-based DAL method hold true:*

$$\left|\left|\left|(u(t^{n+1}) - u_h^{n+1}, \lambda(t^{n+1}) - \lambda_H^{n+1})\right|\right|\right|_p^2 \leq C\left(\frac{h^{1-2\epsilon}H}{\Delta t} + \Delta t\right)\left(\int_0^{t^{n+1}} \left\|\frac{\partial u}{\partial t}\right\|_{H^{3/2-\epsilon}(\Omega)}^2 + \left\|\frac{\partial \lambda}{\partial t}\right\|_{L^2(\Gamma)}^2 + \left\|\frac{\partial^2 u}{\partial t^2}\right\|_{L^2(\Omega)}^2 dt + \|u_0\|_{H^{3/2-\epsilon}(\Omega)}^2 + \|\lambda_0\|_{L^2(\Gamma)}^2\right), \quad (5.68)$$

$$\left\|u(t^{n+1}) - u_h^{n+1}\right\|_{L^2(\Omega)}^2 \leq C(h^{1-2\epsilon}H + \Delta t^2)\left(\int_0^{t^{n+1}} \left\|\frac{\partial u}{\partial t}\right\|_{H^{3/2-\epsilon}(\Omega)}^2 + \left\|\frac{\partial \lambda}{\partial t}\right\|_{L^2(\Gamma)}^2 + \left\|\frac{\partial^2 u}{\partial t^2}\right\|_{L^2(\Omega)}^2 dt + \|u_0\|_{H^{3/2-\epsilon}(\Omega)}^2 + \|\lambda_0\|_{L^2(\Gamma)}^2\right). \quad (5.69)$$

Proof. With the mixed elliptic projection $(\tilde{u}_h(t^{n+1}), \tilde{\lambda}_H(t^{n+1}))$ for $u(t^{n+1})$ and $\lambda(t^{n+1})$, set

$$u(t^{n+1}) - u_h^{n+1} = (u(t^{n+1}) - \tilde{u}_h(t^{n+1})) + (\tilde{u}_h(t^{n+1}) - u_h^{n+1}) = \varphi^{n+1} + \theta^{n+1}, \quad (5.70)$$
$$\lambda(t^{n+1}) - \lambda_H^{n+1} = (\lambda(t^{n+1}) - \tilde{\lambda}_H(t^{n+1})) + (\tilde{\lambda}_H(t^{n+1}) - \lambda_H^{n+1}) = \omega^{n+1} + \xi^{n+1}. \quad (5.71)$$

The estimates of φ^{n+1} and ω^{n+1} are known from Lemma 5.9:

$$\left|\left|\left|(\varphi^{n+1}, \omega^{n+1})\right|\right|\right|_p^2 \leq Ch^{1-2\epsilon}\left(\|u(t^{n+1})\|_{H^{3/2-\epsilon}(\Omega)}^2 + \|\lambda(t^{n+1})\|_{L^2(\Gamma)}^2\right), \quad (5.72)$$
$$\|\varphi^{n+1}\|_{L^2(\Omega)}^2 \leq Ch^{1-2\epsilon}H\left(\|u(t^{n+1})\|_{H^{3/2-\epsilon}(\Omega)}^2 + \|\lambda(t^{n+1})\|_{L^2(\Gamma)}^2\right). \quad (5.73)$$

For θ^{n+1}, taking $w = w_h$ in (4.2) and combining it with the definition of elliptic projection (5.14), one can obtain

$$\left(\left.\frac{\partial u}{\partial t}\right|_{t^{n+1}}, w_h\right) + a\left(\tilde{u}_h(t^{n+1}), w_h\right) + \left\langle\tilde{\lambda}_H(t^{n+1}), w_h\right\rangle + \beta\left\langle\tilde{u}_h(t^{n+1}), w_h\right\rangle = (f(t^{n+1}), w_h) + \beta\left\langle g(t^{n+1}), w_h\right\rangle. \quad (5.74)$$

Subtracting (5.66a) from the above equation yields

$$\begin{aligned}&\left(\overline{\partial}_t\theta^{n+1}, w_h\right) + a(\theta^{n+1}, w_h) + \left\langle\xi^{n+1}, w_h\right\rangle + \beta\left\langle\theta^{n+1}, w_h\right\rangle \\ &= -\left(\overline{\partial}_t\varphi^{n+1}, w_h\right) + \left(\overline{\partial}_t u(t^{n+1}) - \left.\frac{\partial u}{\partial t}\right|_{t^{n+1}}, w_h\right) + \Delta t\left\langle\overline{\partial}_t\xi^{n+1}, w_h\right\rangle + \Delta t\left\langle\overline{\partial}_t\omega^{n+1}, w_h\right\rangle \\ &\quad - \Delta t\left\langle\overline{\partial}_t\lambda(t^{n+1}), w_h\right\rangle. \end{aligned} \quad (5.75)$$

Combining it with lemma 5.8, there exists a $v_h \in X_h$ satisfying

$$\begin{aligned}
&\|\xi^{n+1}\|_{-1/2,h}(\|v_h\|_{H^1(\Omega)} + \|v_h\|_{1/2,h}) \leq C\left\langle \xi^{n+1}, v_h\right\rangle \\
=&C\left(-\left(\overline{\partial}_t\theta^{n+1}, v_h\right) - a(\theta^{n+1}, v_h) - \beta\left\langle\theta^{n+1}, v_h\right\rangle + \Delta t\left\langle\overline{\partial}_t\xi^{n+1}, v_h\right\rangle + \Delta t\left\langle\overline{\partial}_t\omega^{n+1}, v_h\right\rangle\right. \\
&\left.-\Delta t\left\langle\overline{\partial}_t\lambda(t^{n+1}), v_h\right\rangle - \left(\overline{\partial}_t\varphi^{n+1}, v_h\right) + \left(\overline{\partial}_t u(t^{n+1}) - \left.\frac{\partial u}{\partial t}\right|_{t^{n+1}}, v_h\right)\right) \\
\leq&C(\|v_h\|_{H^1(\Omega)} + \|v_h\|_{1/2,h})\left(\|\overline{\partial}_t\theta^{n+1}\|_{L^2(\Omega)} + \|\nabla\theta^{n+1}\|_{L^2(\Omega)} + \|\theta^{n+1}\|_{1/2,h} + \Delta t\|\overline{\partial}_t\xi^{n+1}\|_{-1/2,h}\right. \\
&\left.+\Delta t\|\overline{\partial}_t\omega^{n+1}\|_{-1/2,h} + \Delta t\|\overline{\partial}_t\lambda(t^{n+1})\|_{-1/2,h} + \|\overline{\partial}_t\varphi^{n+1}\|_{L^2(\Omega)} + \left\|\overline{\partial}_t u(t^{n+1}) - \left.\frac{\partial u}{\partial t}\right|_{t^{n+1}}\right\|_{L^2(\Omega)}\right),
\end{aligned}$$

or, equivalently,

$$\begin{aligned}
\|\xi^{n+1}\|^2_{-1/2,h} \leq C_m\left(\right.&\|\overline{\partial}_t\theta^{n+1}\|^2_{L^2(\Omega)} + \|\nabla\theta^{n+1}\|^2_{L^2(\Omega)} + \|\theta^{n+1}\|^2_{1/2,h} + \Delta t^2\|\overline{\partial}_t\xi^{n+1}\|^2_{-1/2,h} \\
&+\Delta t^2\|\overline{\partial}_t\omega^{n+1}\|^2_{-1/2,h} + \Delta t^2\|\overline{\partial}_t\lambda(t^{n+1})\|^2_{-1/2,h} + \|\overline{\partial}_t\varphi^{n+1}\|^2_{L^2(\Omega)} \\
&\left.+\left\|\overline{\partial}_t u(t^{n+1}) - \left.\frac{\partial u}{\partial t}\right|_{t^{n+1}}\right\|^2_{L^2(\Omega)}\right).
\end{aligned} \tag{5.76}$$

On the other hand, for ξ^{n+1}, take $\delta\lambda = \delta\lambda_H$ in (4.2). Then, with the elliptic projection definition (5.14), we have $\left\langle\tilde{u}_h(t^{n+1}) - u(t^{n+1}), \delta\lambda_H\right\rangle = 0$ and $\left\langle\tilde{u}_h(t^{n+1}) - g(t^{n+1}), \delta\lambda_H\right\rangle = 0$. Subtracting (5.66b) from the above equation yields

$$\left\langle\theta^{n+1}, \delta\lambda_H\right\rangle = \frac{\Delta t}{\beta}\left\langle\overline{\partial}_t\xi^{n+1}, \delta\lambda_H\right\rangle - \frac{\Delta t}{\beta}\left\langle\overline{\partial}_t\lambda(t^{n+1}), \delta\lambda_H\right\rangle + \frac{\Delta t}{\beta}\left\langle\overline{\partial}_t\omega^{n+1}, \delta\lambda_H\right\rangle . \tag{5.77}$$

Take $w_h = \theta^{n+1}$ and $\delta\lambda_H = \xi^{n+1}$, subtracting (5.77) from (5.75) yields

$$\begin{aligned}
&\left(\overline{\partial}_t\theta^{n+1}, \theta^{n+1}\right) + a(\theta^{n+1}, \theta^{n+1}) + \frac{\Delta t}{\beta}\left\langle\overline{\partial}_t\xi^{n+1}, \xi^{n+1}\right\rangle + \beta\left\langle\theta^{n+1}, \theta^{n+1}\right\rangle \\
=&-\left(\overline{\partial}_t\varphi^{n+1}, \theta^{n+1}\right) + \left(\overline{\partial}_t u(t^{n+1}) - \left.\frac{\partial u}{\partial t}\right|_{t^{n+1}}, \theta^{n+1}\right) + \Delta t\left\langle\overline{\partial}_t\xi^{n+1}, \theta^{n+1}\right\rangle + \Delta t\left\langle\overline{\partial}_t\omega^{n+1}, \theta^{n+1}\right\rangle \\
&-\Delta t\left\langle\overline{\partial}_t\lambda(t^{n+1}), \theta^{n+1}\right\rangle - \frac{\Delta t}{\beta}\left\langle\overline{\partial}_t\omega^{n+1}, \xi^{n+1}\right\rangle + \frac{\Delta t}{\beta}\left\langle\overline{\partial}_t\lambda(t^{n+1}), \xi^{n+1}\right\rangle .
\end{aligned} \tag{5.78}$$

For the left hand side, we have

$$\begin{aligned}
&\left(\overline{\partial}_t\theta^{n+1}, \theta^{n+1}\right) + a(\theta^{n+1}, \theta^{n+1}) + \frac{\Delta t}{\beta}\left\langle\overline{\partial}_t\xi^{n+1}, \xi^{n+1}\right\rangle + \beta\left\langle\theta^{n+1}, \theta^{n+1}\right\rangle \\
=&\frac{1}{2\Delta t}\left(\|\theta^{n+1}\|^2_{L^2(\Omega)} - \|\theta^n\|^2_{L^2(\Omega)}\right) + \frac{\Delta t}{2}\|\overline{\partial}_t\theta^{n+1}\|^2_{L^2(\Omega)} + \kappa\|\nabla\theta^{n+1}\|^2_{L^2(\Omega)} \\
&+\frac{1}{2l}\left(\|\xi^{n+1}\|^2_{-1/2,h} - \|\xi^n\|^2_{-1/2,h}\right) + \frac{\Delta t^2}{2l}\|\overline{\partial}_t\xi^{n+1}\|^2_{-1/2,h} + l\|\theta^{n+1}\|^2_{1/2,h} .
\end{aligned} \tag{5.79}$$

For the right hand side, when the mesh is strongly regular and $\Delta t \ll 1$ we can combine it

with the inequality (5.76) and obtain

$$
\begin{aligned}
&-\left(\overline{\partial}_t\varphi^{n+1},\theta^{n+1}\right)+\left(\overline{\partial}_t u(t^{n+1})-\left.\frac{\partial u}{\partial t}\right|_{t^{n+1}},\theta^{n+1}\right)+\Delta t\left\langle\overline{\partial}_t\xi^{n+1},\theta^{n+1}\right\rangle+\Delta t\left\langle\overline{\partial}_t\omega^{n+1},\theta^{n+1}\right\rangle\\
&-\Delta t\left\langle\overline{\partial}_t\lambda(t^{n+1}),\theta^{n+1}\right\rangle-\frac{\Delta t}{\beta}\left\langle\overline{\partial}_t\omega^{n+1},\xi^{n+1}\right\rangle+\frac{\Delta t}{\beta}\left\langle\overline{\partial}_t\lambda(t^{n+1}),\xi^{n+1}\right\rangle\\
\leq&\frac{\kappa}{2C_{\mathrm{Po}}}\|\theta^{n+1}\|^2_{L^2(\Omega)}+\frac{C_{\mathrm{Po}}}{\kappa}\|\overline{\partial}_t\varphi^{n+1}\|^2_{L^2(\Omega)}+\frac{C_{\mathrm{Po}}}{\kappa}\left\|\overline{\partial}_t u(t^{n+1})-\left.\frac{\partial u}{\partial t}\right|_{t^{n+1}}\right\|^2_{L^2(\Omega)}+\frac{\Delta t^2}{3l}\left\|\overline{\partial}_t\xi^{n+1}\right\|^2_{-1/2,h}\\
&+\frac{3l}{4}\|\theta^{n+1}\|^2_{1/2,h}+\frac{\Delta t}{2}\|\theta^{n+1}\|^2_{1/2,h}+\Delta t\|\overline{\partial}_t\omega^{n+1}\|^2_{-1/2,h}+\Delta t\|\overline{\partial}_t\lambda(t^{n+1})\|^2_{-1/2,h}+\frac{\Delta t}{4C_m}\|\xi^{n+1}\|^2_{-1/2,h}\\
&+\frac{2\Delta tC_m}{l^2}\|\overline{\partial}_t\omega^{n+1}\|^2_{-1/2,h}+\frac{2\Delta tC_m}{l^2}\|\overline{\partial}_t\lambda(t^{n+1})\|^2_{-1/2,h}\\
\leq&\frac{\kappa}{2}\|\nabla\theta^{n+1}\|^2_{L^2(\Omega)}+\frac{C_{\mathrm{Po}}}{\kappa}\|\overline{\partial}_t\varphi^{n+1}\|^2_{L^2(\Omega)}+\frac{C_{\mathrm{Po}}}{\kappa}\left\|\overline{\partial}_t u(t^{n+1})-\left.\frac{\partial u}{\partial t}\right|_{t^{n+1}}\right\|^2_{L^2(\Omega)}+\frac{\Delta t^2}{3l}\left\|\overline{\partial}_t\xi^{n+1}\right\|^2_{-1/2,h}\\
&+\frac{3l}{4}\|\theta^{n+1}\|^2_{1/2,h}+\frac{\Delta t}{4}\|\overline{\partial}_t\theta^{n+1}\|^2_{L^2(\Omega)}+\frac{\Delta t(l^2+2C_m)}{l^2}\|\overline{\partial}_t\omega^{n+1}\|^2_{-1/2,h}+\frac{\Delta t(l^2+2C_m)}{l^2}\|\overline{\partial}_t\lambda(t^{n+1})\|^2_{-1/2,h}\,.
\end{aligned}
$$

Note that we have employed the consequence of the Poincaré's inequality, specifically, $\|\theta^{n+1}\|^2_{L^2(\Omega)}\leq C_{\mathrm{Po}}\|\nabla\theta^{n+1}\|^2_{L^2(\Omega)}$. Putting the inequalities for the left hand side and the right hand side together, (5.78) yields

$$
\begin{aligned}
&\left(\|\theta^{n+1}\|^2_{L^2(\Omega)}-\|\theta^{n}\|^2_{L^2(\Omega)}\right)+\frac{\Delta t^2}{2}\|\overline{\partial}_t\theta^{n+1}\|^2_{L^2(\Omega)}+\kappa\Delta t\|\nabla\theta^{n+1}\|^2_{L^2(\Omega)}+\frac{\Delta t}{l}\left(\|\xi^{n+1}\|^2_{-1/2,h}-\|\xi^{n}\|^2_{-1/2,h}\right)\\
&+\frac{\Delta t^3}{3l}\|\overline{\partial}_t\xi^{n+1}\|^2_{-1/2,h}+\frac{\Delta tl}{2}\|\theta^{n+1}\|^2_{1/2,h}\\
\leq&C\left(\Delta t\|\overline{\partial}_t\varphi^{n+1}\|^2_{L^2(\Omega)}+\Delta t\left\|\overline{\partial}_t u(t^{n+1})-\left.\frac{\partial u}{\partial t}\right|_{t^{n+1}}\right\|^2_{L^2(\Omega)}+\Delta t^2\|\overline{\partial}_t\omega^{n+1}\|^2_{-1/2,h}+\Delta t^2\|\overline{\partial}_t\lambda(t^{n+1})\|^2_{-1/2,h}\right)\,.
\end{aligned}
$$

The terms in the right hand side can be bounded as

$$
\begin{aligned}
&\|\overline{\partial}_t\varphi^{n+1}\|^2_{L^2(\Omega)}\leq\frac{1}{\Delta t}\int_{t^n}^{t^{n+1}}\left\|\frac{\partial\varphi}{\partial t}\right\|^2_{L^2(\Omega)}dt\leq\frac{Ch^{1-2\epsilon}H}{\Delta t}\int_{t^n}^{t^{n+1}}\left(\left\|\frac{\partial u}{\partial t}\right\|^2_{H^{3/2-\epsilon}(\Omega)}+\left\|\frac{\partial\lambda}{\partial t}\right\|^2_{L^2(\Gamma)}\right)dt,\\
&\left\|\overline{\partial}_t u(t^{n+1})-\left.\frac{\partial u}{\partial t}\right|_{t^{n+1}}\right\|^2_{L^2(\Omega)}\leq\Delta t\int_{t^n}^{t^{n+1}}\left\|\frac{\partial^2 u}{\partial t^2}\right\|^2_{L^2(\Omega)}dt,\\
&\|\overline{\partial}_t\omega^{n+1}\|^2_{-1/2,h}\leq\frac{1}{\Delta t}\int_{t^n}^{t^{n+1}}\left\|\frac{\partial\omega}{\partial t}\right\|^2_{-1/2,h}dt\leq\frac{Ch^{1-2\epsilon}}{\Delta t}\int_{t^n}^{t^{n+1}}\left(\left\|\frac{\partial u}{\partial t}\right\|^2_{H^{3/2-\epsilon}(\Omega)}+\left\|\frac{\partial\lambda}{\partial t}\right\|^2_{L^2(\Gamma)}\right)dt,\\
&\|\overline{\partial}_t\lambda(t^{n+1})\|^2_{-1/2,h}\leq\frac{Ch}{\Delta t}\int_{t^n}^{t^{n+1}}\left\|\frac{\partial\lambda}{\partial t}\right\|^2_{L^2(\Gamma)}dt.
\end{aligned}
$$

Combining with $h\ll 1$, $h<H$ and summing up from the first step to the $(n+1)^{\mathrm{st}}$ step, the

above bounds and the fact $h^{1-2\epsilon}\Delta t \le C(h^{2-4\epsilon}+\Delta t^2) \le C(h^{1-2\epsilon}H+\Delta t^2)$ lead to

$$\begin{aligned}
&\|\theta^{n+1}\|^2_{L^2(\Omega)} + \frac{\Delta t^2}{2}\sum_{i=0}^{n}\|\overline{\partial}_t\theta^{i+1}\|^2_{L^2(\Omega)} + \kappa\Delta t\sum_{i=0}^{n}\|\nabla\theta^{i+1}\|^2_{L^2(\Omega)} + \frac{\Delta t}{l}\|\xi^{n+1}\|^2_{-1/2,h} + \frac{\Delta t^3}{3l}\sum_{i=0}^{n}\|\overline{\partial}_t\xi^{i+1}\|^2_{-1/2,h}\\
&+\frac{\Delta t l}{2}\sum_{i=0}^{n}\|\theta^{i+1}\|^2_{1/2,h}\\
\le& C(h^{1-2\epsilon}H+\Delta t^2)\int_0^{t^{n+1}}\left\|\frac{\partial u}{\partial t}\right\|^2_{H^{3/2-\epsilon}(\Omega)} + \left\|\frac{\partial\lambda}{\partial t}\right\|^2_{L^2(\Gamma)} + \left\|\frac{\partial^2 u}{\partial t^2}\right\|^2_{L^2(\Omega)} dt + \|\theta^0\|^2_{L^2(\Omega)} + \frac{\Delta t}{l}\|\xi^0\|^2_{-1/2,h}.
\end{aligned}$$

While taking the initial values of u_h^0 and λ_H^0 as in (5.66), we have estimates for the initial errors:

$$\begin{aligned}
&\|\theta^0\|^2_{L^2(\Omega)} \le C(\|\tilde{u}_h(0)-u_0\|^2_{L^2(\Omega)} + \|u_0 - I_h u_0\|^2_{L^2(\Omega)}) \le Ch^{1-2\epsilon}H(\|u_0\|^2_{H^{3/2-\epsilon}(\Omega)} + \|\lambda_0\|^2_{L^2(\Gamma)}),\\
&\|\xi^0\|^2_{-1/2,h} \le C(\|\tilde{\lambda}_H(0)-\lambda(0)\|^2_{-1/2,h} + 2\|\lambda(0)\|^2_{-1/2,h}) \le Ch^{1-2\epsilon}(\|u_0\|^2_{H^{3/2-\epsilon}(\Omega)} + \|\lambda_0\|^2_{L^2(\Gamma)}).
\end{aligned}$$

Substituting the initial error estimates gives

$$\begin{aligned}
&\|\theta^{n+1}\|^2_{L^2(\Omega)} + \frac{\Delta t^2}{2}\sum_{i=0}^{n}\|\overline{\partial}_t\theta^{i+1}\|^2_{L^2(\Omega)} + \kappa\Delta t\sum_{i=0}^{n}\|\nabla\theta^{i+1}\|^2_{L^2(\Omega)} + \frac{\Delta t}{l}\|\xi^{n+1}\|^2_{-1/2,h}\\
&+\frac{\Delta t^3}{3l}\sum_{i=0}^{n}\|\overline{\partial}_t\xi^{i+1}\|^2_{-1/2,h} + \frac{\Delta t l}{2}\sum_{i=0}^{n}\|\theta^{i+1}\|^2_{1/2,h}\\
\le& C(h^{1-2\epsilon}H+\Delta t^2)\left(\int_0^{t^{n+1}}\left\|\frac{\partial u}{\partial t}\right\|^2_{H^{3/2-\epsilon}(\Omega)} + \left\|\frac{\partial\lambda}{\partial t}\right\|^2_{L^2(\Gamma)} + \left\|\frac{\partial^2 u}{\partial t^2}\right\|^2_{L^2(\Omega)} dt\right.\\
&\left.+\|u_0\|^2_{H^{3/2-\epsilon}(\Omega)} + \|\lambda_0\|^2_{L^2(\Gamma)}\right),
\end{aligned} \tag{5.80}$$

which yields the estimate for θ^{n+1} in the L^2 norm. Combining it with the estimate for φ^{n+1}, we obtain the error estimate in the L^2 norm. On the other hand, from (5.80), we have also obtained

$$\begin{aligned}
&\|\nabla\theta^{n+1}\|^2_{L^2(\Omega)} + \|\theta^{n+1}\|^2_{1/2,h} + \|\xi^{n+1}\|^2_{-1/2,h}\\
\le& C\left(\frac{h^{1-2\epsilon}H}{\Delta t}+\Delta t\right)\left(\|u_0\|^2_{H^{3/2-\epsilon}(\Omega)} + \|\lambda_0\|^2_{L^2(\Gamma)} + \int_0^{t^{n+1}}\left\|\frac{\partial u}{\partial t}\right\|^2_{H^{3/2-\epsilon}(\Omega)} + \left\|\frac{\partial\lambda}{\partial t}\right\|^2_{L^2(\Gamma)} + \left\|\frac{\partial^2 u}{\partial t^2}\right\|^2_{L^2(\Omega)} dt\right).
\end{aligned}$$

Together with the estimates for φ^{n+1} and ω^{n+1}, we have obtained the error estimate in the $|||(\cdot,\cdot)|||_p$-norm, and therefore have finished the error estimate of the projection-based DAL method. □

Theorem 5.2 has indicated the following corollary:

Corollary 5.1. *In the projection-based fully-discrete DAL method, the optimal time step size is $\Delta t = O(h) = O(H)$, which yields the error estimates:*

$$\|\nabla(u(t^n)-u_h^n)\|_{L^2(\Omega)} + \|u(t^n)-u_h^n\|_{1/2,h} + \|\lambda(t^n)-\lambda_h^n\|_{-1/2,h} \le Ch^{1/2-\epsilon}, \tag{5.81}$$

$$\|u(t^n)-u_h^n\|_{L^2(\Omega)} \le Ch^{1-\epsilon}. \tag{5.82}$$

Or, equivalently, $h^{1/2-\epsilon}$ order of accuracy for the $|||(\cdot,\cdot)|||_p$-norm and $h^{1-\epsilon}$ order for u in the $L^2(\Omega)$-norm.

Remark 5.4. Due to the lack of strong consistency of the method and the problem regularity in the static problem, we lose $h^{1/2+\epsilon}$ order for the $|||(\cdot,\cdot)|||$-norm and $h^{1+\epsilon}$ order for the L^2-norm, as shown in (5.52) and (5.53).

Remark 5.5. Given the problem regularity $u \in H^{3/2-\epsilon}(\Omega)$, the above error estimates are consistent with the error estimates in [22]. Therefore, although the original augmented Lagrangian iteration was truncated in the DAL methods, the error estimates have shown that comparing with the algorithms in [22] where the Lagrange multiplier was updated exactly, such a truncation in the iterations did not affect the convergence rates for u, due to the fact that the error introduced by this truncation is actually of the same order with the error from the degraded solution regularity.

Remark 5.6. The $\dfrac{h^{1-2\epsilon}H}{\Delta t}$ term in (5.68) suggests that, when taking Δt smaller than $O(hH)$, one might expect to see large errors in the H^1-norm. A similar concern was raised by the earlier analysis of [35]. However, numerical experiments in section 6.4 suggest that the method remains robust in the limit of temporal over-refinement.

6. Numerical results for model problems

In this section, we test the results of the analysis for the projection-based DAL method, then explore how robust the results are by applying them in situations outside the scope of the linearized model problem analysis presented earlier. In section 6.1 and section 6.2, the projection-based DAL method with two types of element spaces for the Lagrange multiplier W_H are investigated. Moreover, in section 6.3 we demonstrate the kinematic conservation property of the projection-based DAL method, which was the original motivation for developing this method. Lastly, in section 6.4 we investigate the stability of the temporal over-refinement cases as discussed in Remark 5.6. To demonstrate the robustness, in section 6.4 we employ the projection-based DAL method with $W_H = W_h$, which represents the case with the worst stability among the DAL methods.

6.1. *Confirming estimates: foreground definition for W_H*

To test the conclusions of our error analysis for the projection-based DAL method, we construct a particular linearized model problem. We set the space dimension to two and choose $a(u,v) = (\nabla u, \nabla v)_{L^2(\Omega)}$. Ω is the square $(-W/2, W/2)^2 \subset \mathbb{R}^2$, with $W = 2.5$, and Γ is the unit circle $\{\mathbf{x} \in \mathbb{R}^2 \ : \ \|\mathbf{x}\|_{\ell^2} = 1\}$. The time interval terminates at $T = 0.1$. The initial temperature distribution is

$$u_0(\mathbf{x}) = u_{\text{Bess}}(\mathbf{x}) + u_{\sin}(\mathbf{x}) \,, \tag{6.1}$$

where

$$u_{\text{Bess}}(\mathbf{x}) = \begin{cases} J_0\left(R\|\mathbf{x}\|_{\ell^2}\right) & \|\mathbf{x}\|_{\ell^2} < 1 \\ 0 & \text{otherwise} \end{cases} \tag{6.2}$$

and

$$u_{\sin}(\mathbf{x}) = \sin\left(\frac{2\pi x_1}{W}\right)\sin\left(\frac{2\pi x_2}{W}\right), \tag{6.3}$$

where R is the first root of the Bessel function J_0. Given $g = u|_\Gamma$ and $f = 0$, this problem has a time-dependent analytic solution as

$$u(\mathbf{x}, t) = u_{\text{Bess}}(\mathbf{x})e^{-R^2 t} + u_{\sin}(\mathbf{x})e^{-\left(\frac{8\pi^2 t}{W^2}\right)}. \tag{6.4}$$

This solution exhibits discontinuous first derivatives of u at Γ and is smooth everywhere else, i.e., $u \in H^{3/2-\epsilon}(\Omega)$; this matches the spatial regularity that is shown to hold over a large class of problem data in Section 4. The exact multiplier λ is constant in space and decaying in time, corresponding to the jump in normal derivative of the Bessel function component of u.[a]

To define the space $W_H(\Gamma)$, in this section we divide Γ into elements of size $\sim H$, as illustrated in the left plot of Figure 2. In the following developments, we denote this type of definition for W_H as the "foreground" construction [36]. In contrast with the "foreground" construction in this section, in the right plot of Figure 2 we illustrate another choice of Lagrange multiplier space construction, i.e., the "background" construction. In the background construction, the Lagrange multiplier is discretized in the trace on Γ of a space of degree-zero B-splines with every other knot's multiplicity set to zero along each direction (i.e. the space of constants on clusters of 2^d Bézier elements, see [36] for further details), and its numerical performance will be discussed in the next section.

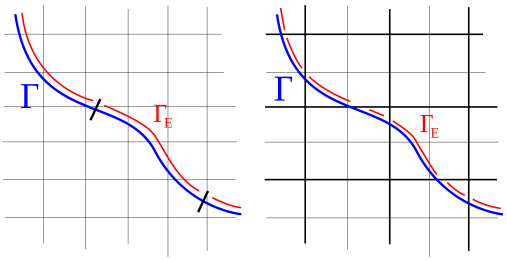

Fig. 2. Sketches illustrating foreground (left) and background (right) definitions of the boundary Lagrange multiplier. In each case, Γ_E indicates a section of Γ that serves as an element domain in the multiplier mesh.

We now discretize the temperature field with a linear uniform B-spline space of $2^M \times 2^M$ elements, for $M \in \{3, \ldots, 11\}$. The Lagrange multiplier is approximated with a piecewise constant function on 2^{M-3} elements that evenly divide the arc length of Γ, i.e., λ_H is represented with a single constant element in the computations with the coarsest 8×8 background mesh ($M = 3$), and a constant ratio of H/h is maintained during refinement.

[a]Although the exact multiplier is trivial to represent with any reasonable discrete space, we expect the discrete solution to be polluted by errors in u, as indicated by the bounds derived previously.

Defining $H = 2\pi/(2^{M-3})$, i.e., the arc length of one element, $H/h \approx 20$. If we take H to be the arc length of one of these elements and let $h = W/2^M$, then we have $H \sim h$. We set $\beta = 1/h$. The discrete initial condition is set by nodal interpolation of u_0. Integrals over Γ are evaluated using 32×2^M evenly-spaced quadrature points. The time step is proportional to h, viz. $\Delta t = T/2^M$. An illustrative snapshot of a numerical solution is shown in Figure 3.

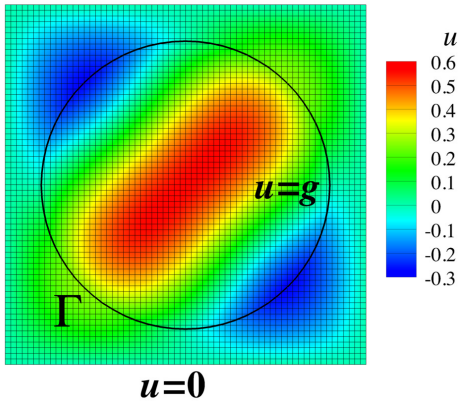

Fig. 3. Annotated snapshot of a numerical solution to the scalar parabolic test problem.

The convergence results of projection-based DAL method are illustrated in Figure 4. The left plot of Figure 4 shows the convergence of the $L^2(\Omega)$ and $H^1(\Omega)$ norms of the error $u(T) - u_h^N$, suggesting convergence rates of 1/2 in $H^1(\Omega)$ and 1 in $L^2(\Omega)$ for both cases, as expected from the analysis. The right plot of Figure 4 shows the convergence of the $L^2(\Gamma)$ norm of the multiplier error $\lambda_H - \lambda$ at time T. Although this error does not diverge, it is only bounded under refinement. This observation is consistent with convergence at a rate of $1/2$ in the weaker $\|\cdot\|_{-1/2,h}$ norm.

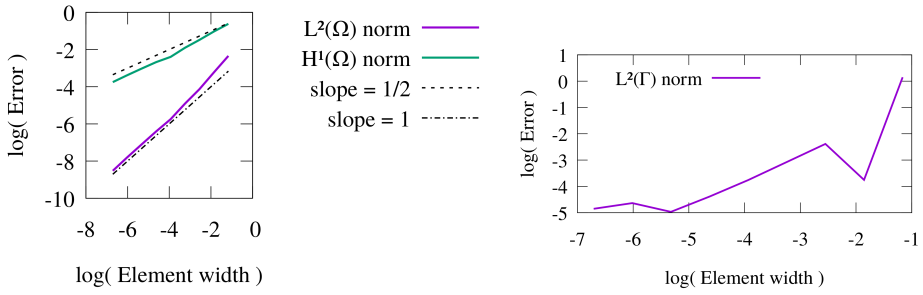

Fig. 4. Convergence of u and λ while using a foreground-mesh-derived multiplier space in the projection-based DAL method, with respect to element size h and $\Delta t = O(h)$. Left: $L^2(\Omega)$ and $H^1(\Omega)$ errors of $u(T)$. Right: $L^2(\Gamma)$ error of $\lambda(T)$.

The lack of convergence of the Lagrange multiplier in a strong norm is also clear from comparing plots of the Lagrange multiplier at various levels of refinement. The multiplier field $\lambda(T)$ is shown at several refinement levels in Figure 5, as a function of the arc length along Γ. While there is an obvious improvement from the coarsest discretizations to more refined ones, the magnitudes of oscillations in the asymptotic regime do not decrease, as is consistent with the $O(1)$ $L^2(\Gamma)$ error shown in the right plot of Figure 4.

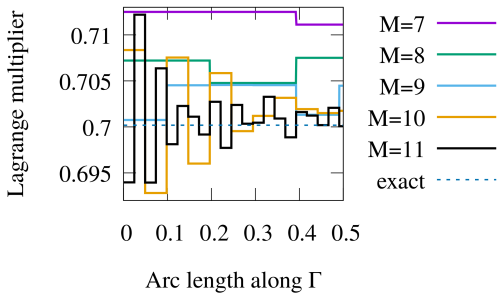

Fig. 5. The Lagrange multiplier as a function of arc length along Γ, at various levels M of refinement, when using the foreground mesh to define W_H.

6.2. *Confirming estimates: background definition for W_H*

It would at first appear very intuitive to define the space $W_H(\Gamma)$ by dividing Γ into elements of size $\sim H$, as in the numerical experiments of Section 6.1. However, this use of a "foreground" construction may lead to difficulties in practice. In the FSI case, one might immerse a structure into a background mesh of the fluid domain that is refined in a highly non-uniform and/or anisotropic way, to, e.g., capture boundary layers near a fitted boundary. A foreground construction of W_H that is appropriate for a structure immersed in one part of Ω may become inappropriate as the structure moves to a less-refined region or changes its orientation relative to anisotropic refinement of the background mesh. Puso et al. [98] previously compared foreground and background definitions of Lagrange multiplier spaces for immersed discretizations and found that defining the Lagrange multiplier using the background mesh was typically a more stable choice. In [36], a background-based definition of the Lagrange multiplier was employed for isogeometric background discretizations, which will be investigated in this section.

We now test the convergence of the projection-based DAL method with this background multiplier space. Aside from changing the definition of W_H, we repeat the experiment of Section 6.1. The convergence of the error in temperature is shown in the left plot of Figure 6; we obtain the same convergence rates as we did when using the foreground multiplier space. The $O(1)$ $L^2(\Gamma)$ error for the multiplier λ, shown in the right plot of Figure 6, is also consistent with the results of Section 6.1.

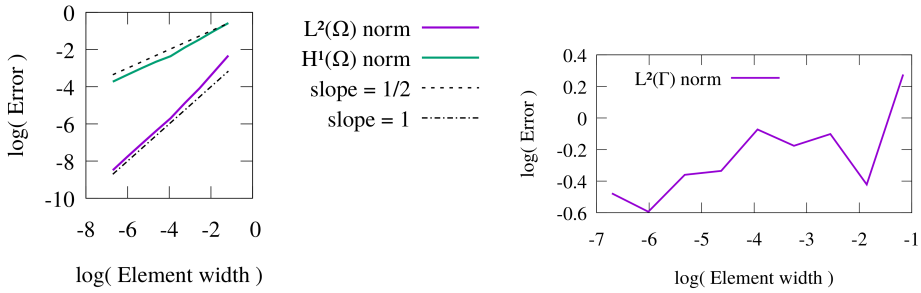

Fig. 6. Convergence results of u and λ while using a background-mesh-derived multiplier space in the projection-based DAL method, with respect to element size h and $\Delta t = O(h)$. Left: convergence of of $L^2(\Omega)$ and $H^1(\Omega)$ errors of $u(T)$. Right: convergence of the $L^2(\Gamma)$ error of $\lambda(T)$.

The multiplier field in this case appears to have oscillations of larger amplitude, as shown in Figure 7. The thin spikes in Figure 7 correspond to poorly cut elements of the background mesh which would possibly violate the quasi-uniform assumption of W_H and cause numerical instabilities. While these oscillations and spikes may look alarming, they do not appear to impede the convergence of the temperature solution. Further, unlike multiplier oscillations in the $r = 0$ limit of the DAL method from [34], these spurious features do not grow in an unbounded way under temporal refinement, or in the limit of $T \to \infty$.

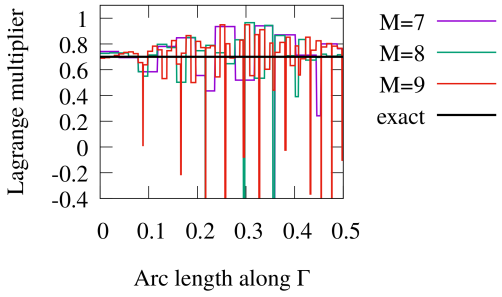

Fig. 7. The Lagrange multiplier as a function of arc length along Γ, at various levels M of refinement, when using the background mesh to define W_H. Note that some of the functions plotted extend beyond the bounds on the vertical axis.

6.3. *Advantages of the projection-based DAL method*

As elaborated in [36], the purpose of the projection-based DAL method is to ensure kinematic conservation in the steady limit without needing to reduce the constraint regularization parameter r to an unstable value near zero. We demonstrate this conservation property

on the problem introduced in Section 6.1 by looking at the conservation error (cf. (3.3))

$$E_\Gamma = \int_\Gamma \left(u_h^N - g(T) \right) d\Gamma \tag{6.5}$$

in the limit of $\Delta t \to 0$ at fixed h. We use the $M = 4$ meshes of Ω and Γ defined in Section 6.1 and consider $\Delta t = T/2^{M_t}$, for $M_t \in \{3, \ldots, 10\}$. For computations we compare the results of $\log |E_\Gamma|$ from the projection-based DAL method with the results using the DAL method from [34] with $r = 1$. The resulting values of $\log |E_\Gamma|$ are plotted in Figure 8. It is clear that the projection-based DAL recovers kinematic conservation, with the conservation error converging as $O(\Delta t)$, while the conservation error from the original DAL does not converge.

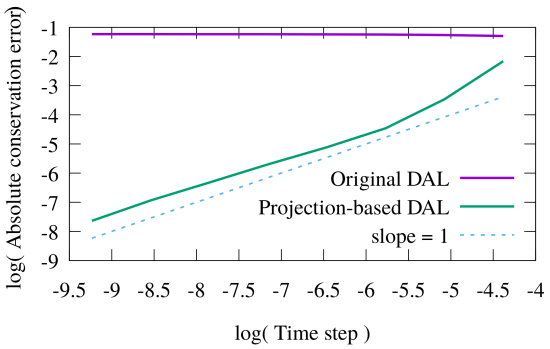

Fig. 8. Convergence of $\log |E_\Gamma|$ as $\Delta t \to 0$ at fixed h.

6.4. *Over-refinement in time*

As mentioned in Remark 5.6, error estimates suggest a lower bound for stability on the time step in terms of h and H as $\Delta t \geq O(h^{1-2\epsilon} H)$. The possibility of error blowing up under temporal refinement is a serious practical concern in nonlinear FSI simulations, as reducing Δt on a fixed spatial discretization may be necessary to ensure stability or rapid convergence. (See, e.g., the stability analysis in [35, Section 4] of the block iterative procedure used to resolve the implicit step of the time integrator.) In this section, we explore the consequences of refining too quickly in time, relative to the spatial discretization.

To exacerbate the potential small-time-step instability, we consider the projection-based DAL method with limiting case of $W_H = W_h$ and run two experiments using the scalar parabolic model problem. First, we refine in both space and time, with $\Delta t \sim h^2$. Then, we refine in time while holding h fixed. Based on the bound (5.68), we might expect to see $H^1(\Omega)$ errors in temperature fail to converge in the first case, and diverge in the second case. The particular problem we consider is the same as that used in Section 6.1. We use (part of) the same sequence of spatial meshes for the temperature field, and attempt to cast a spotlight on any possible unstable behavior of the multiplier by setting $\beta = 10^5/h$.

The convergence of error in temperature at time T is shown for $\Delta t = T/(2^M/4)^2$ in the left plot of Figure 9. The temperature error when taking $\Delta t \to 0$ on the $M = 4$ spatial mesh is shown in the right plot of Figure 9. We see from these results that the apparent small-time-step divergence of the error bound (5.68) appears to be a false alarm, suggesting that either the predicted divergence only occurs in select pathological cases, or the theoretical estimate is overly pessimistic.

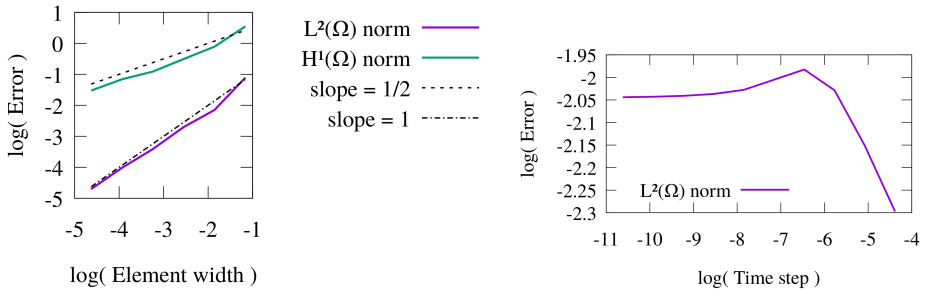

Fig. 9. Convergence results of u with over-refinement in time, with the projection-based DAL method and $\beta = 10^5/h, W_H = W)h$. Left: Convergence of $L^2(\Omega)$ and $H^1(\Omega)$ errors in $u(T)$ when taking $\Delta t \sim h^2$. Right: Convergence of $L^2(\Omega)$ error in $u(T)$ when taking $\Delta t \to 0$ at fixed h. (For h fixed, all norms of u_h^N are equivalent.)

7. A benchmark problem and numerical results for nonlinear FSI

In this section we test how well the model problem analysis extrapolates to the setting of nonlinear FSI, on a benchmark 2D FSI problem with manufactured solution. Briefly, we first derived a benchmark problem with analytic solution that exhibits the regularity expected in practice and satisfies all kinematic constraints, then substituting it into the strong form of the governing equations, to obtain a source term. This is complicated by several factors in the case of unsteady fluid–thin structure interaction. First, the overall method presumes that the solution is stable, but this cannot be assured in nonlinear problems, especially with thin structures (that may buckle) and fluid flow (that may become turbulent). Second, the expected regularity of the fluid solution in immersed FSI applications is less than that needed by the strong form of the governing equations.

We address the first of these challenges by considering flow at low Reynolds numbers, to avoid turbulence, and formulating the thin structure as a prestressed membrane. In particular, we select the constitutive law of the structure in (2.8) to be

$$\int_{-h_{\rm th}/2}^{h_{\rm th}/2} D_{\mathbf{w}}\mathbf{E} : \mathbf{S}\, d\xi = \int_{-h_{\rm th}/2}^{h_{\rm th}/2} D_{\mathbf{w}}\boldsymbol{\varepsilon} : (\mathbf{n} + \mathbf{n}^{\rm pre})\, d\xi\,, \tag{7.1}$$

where $\boldsymbol{\varepsilon}$ is membrane strain [80, (3.34)], $\mathbf{n}$ is the membrane resultant force [80, (3.38)], and $\mathbf{n}^{\rm pre}$ is a prescribed membrane prestress (cf. [99, (5)], in the 3D solid setting). To resolve the second difficulty, we construct the benchmark problem in the way that the distributional

parts of the fluid solution derivatives are always induced by fluid–structure coupling, rather than imposed in the manufacturing process, through an artificial concentrated source term. To be specific, the benchmark 2D FSI problem is constructed through the following steps: In Section 7.1, define the shell structure displacement, and define a solenoidal fluid velocity field with a discontinuous gradient at the deformed shell structure position. Then calculate the body force $\mathbf{f}_1$ on the fluid from the strong form of the fluid equation. In Section 7.2, compute the jump in fluid traction, $-\boldsymbol{\lambda}$, at the shell structure, due to the jump in velocity gradient and an arbitrary pressure difference. In Section 7.3, prescribe $-\boldsymbol{\lambda}$ as a fixed traction on the structure, then solve for the remaining body force, $\mathbf{f}_2$, based on the strong form of the shell equation. Lastly, in Section 7.4 we test the convergence of the computational results from the projection-based DAL method in the derived benchmark 2D FSI problem, with respect to the manufactured analytic solution.

7.1. *Choosing structure displacement and velocity solutions*

The fluid subproblem domain is $\Omega = (0, L)^2$ and the initial shell structure midsurface divides Ω in half: $\Gamma_0 = \{L/2\} \times (0, L)$. We parameterize this midsurface by $\xi_1 = X_2$, so that the conversion between curvilinear and local Cartesian coordinates in the reference configuration [80, (3.41)] is simple. We want to manufacture a shell structure displacement solution

$$\mathbf{y}(\mathbf{X}, t) = VtY(X_2)\mathbf{e}_1 \text{ ,where } V > 0 \text{ and } Y(x) = x(L - x) = Lx - x^2. \tag{7.2}$$

Note that the expression for $\mathbf{y}$ remains well-defined for $\mathbf{X} \notin \Gamma_0$, which will be useful in the construction of the conforming fluid velocity field. A sketch of the problem is shown in the left plot of Figure 10.

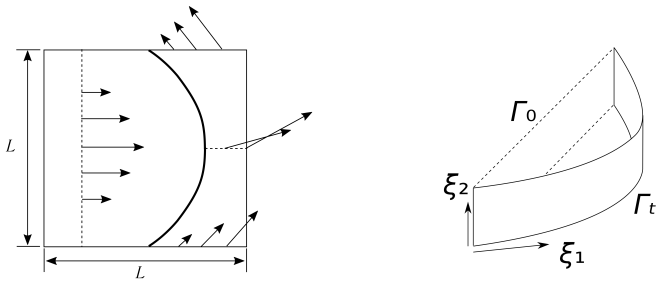

Fig. 10. A sketch of the benchmark FSI problem settings. Left: The fluid domain with the deformed structure, where arrows indicate the surrounding fluid velocity field. Right: Shell structure parameterization.

Remark 7.1. If bending is included in the shell structure, one can avoid issues with the time-dependent boundary condition on the shell structure bending moment by replacing the $Y(x)$ in (7.2) with $Y(x) = \frac{1}{2}\left(1 - \cos\left(\frac{2\pi x}{L}\right)\right)$ or some other function for which $Y'(0) = Y'(L) = 0$.

The fluid velocity field must conform to the selected structure displacement. Further, to have regularity representative of expected applications, we want the pressure and fluid velocity gradients to be discontinuous at Γ_t. For $\mathbf{x} \in \Omega$ with $x_1 < L/2 + VtY(x_2)$ (i.e., $\mathbf{x}$ is to the left of Γ_t), we set

$$\mathbf{u}^{\text{left}}(\mathbf{x}, t) = VY(x_2)\mathbf{e}_1 \,. \tag{7.3}$$

On the other hand, for $\mathbf{x}$ to the right of Γ_t,

$$\mathbf{u}^{\text{right}}(\mathbf{x}, t) = VY(x_2)\mathbf{e}_1 + \mathbf{u}_{\text{shear}}(\mathbf{x}, t) \,, \tag{7.4}$$

with

$$\mathbf{u}_{\text{shear}}(\mathbf{x}, t) = \mathbf{F}\left(\phi^{-1}(\mathbf{x}, t)\right)\mathbf{U}_{\text{shear}}\left(\phi^{-1}(\mathbf{x}), t\right) = \frac{V(x_1 - (VtY(x_2) + L/2))}{L}\left(VtY'(x_2)\mathbf{e}_1 + \mathbf{e}_2\right).$$

The fluid and structure solutions can then be manufactured by taking derivatives $\nabla\mathbf{u}$, $\Delta\mathbf{u}$, and $\partial_t\mathbf{u}$ to the left and right sides of the (deformed) structure, i.e., (7.3) and (7.4). Specifically, we calculate the body force term for the whole fluid domain

$$\rho_f\mathbf{f}_1 = \rho_f\left(\partial_t\mathbf{u} + \mathbf{u}\cdot\nabla\mathbf{u}\right) - \mu\Delta\mathbf{u} - \nabla p \,, \tag{7.5}$$

where ∇p is an arbitrary irrotational pressure gradient. For simplicity, we assume that $\nabla p = 0$ to the left and right of the structure, with a pressure jump P across the deformed structure Γ_t, i.e., $p^{\text{left}} - p^{\text{right}} = P$.

7.2. *Obtaining the traction jump on the structure*

We can now prescribe the fluid traction jump across the structure as a source term on the structure. With the gradient $\nabla\mathbf{u}$ computed above, we can write the viscous stress in the fluid as a function of the shell structure midsurface parameter ξ_1:

$$\boldsymbol{\tau}\left(\xi_1, t\right) = \mu\left(\nabla\mathbf{u}\left(\mathbf{X}(\xi_1) + \mathbf{y}(\xi_1, t)\right) + \left(\nabla\mathbf{u}\left(\mathbf{X}(\xi_1) + \mathbf{y}(\xi_1, t)\right)\right)^T\right). \tag{7.6}$$

We now set the fluid-induced traction load on the structure subproblem as:

$$-\boldsymbol{\lambda} = \left(\boldsymbol{\tau}^{\text{right}}\mathbf{n}_s - \boldsymbol{\tau}^{\text{left}}\mathbf{n}_s\right) + P\mathbf{n}_s \text{ , where } \mathbf{n}_s = \frac{1}{\sqrt{1 + (VtY')^2}}\begin{pmatrix} 1 \\ -VtY' \end{pmatrix}, \tag{7.7}$$

and P is the pressure jump.

7.3. *Manufacturing the shell structure solution*

We now manufacture a shell structure solution by determining the remaining prescribed forcing needed to obtain the solution $\mathbf{y} = VtY(X_2)\mathbf{e}_1$ in the presence of the exact fluid subproblem solution. To apply shell theory to a 1D structure, consider it to be extruded in the x_3 direction, along which all problem variables are constant, as illustrated in the right plot of Figure 10.

We need to first derive the Euler–Lagrange form of the shell structure's virtual work principle. To define the membrane strain, we define the covariant basis vectors in the reference and current configurations:

$$\text{In the reference configuration:} \quad \mathbf{A}_1 = \mathbf{e}_2 \quad , \quad \mathbf{A}_2 = \mathbf{e}_3 \, ,$$

$$\text{In the current configuration:} \quad \mathbf{a}_1 = \frac{\partial \mathbf{x}}{\xi_1} = \begin{pmatrix} VtY' \\ 1 \end{pmatrix} \quad , \quad \mathbf{a}_2 = \mathbf{A}_2 \, .$$

The midsurface metric tensor in the reference configuration is identity due to the choice of a Cartesian parameterization. The (pulled-back) midsurface metric tensor in the deformed configuration is

$$g_{\alpha\beta}\mathbf{A}^\alpha \otimes \mathbf{A}^\beta = \begin{pmatrix} \left(1 + (VtY')^2\right) & 0 \\ 0 & 1 \end{pmatrix} , \tag{7.8}$$

where $\mathbf{A}^\alpha$ are the contravariant basis vectors such that $\mathbf{A}_\alpha \cdot \mathbf{A}^\beta = \delta_\alpha{}^\beta$. Since the displacements in the x_3-direction are constrained to be zero, the membrane strain is then

$$\varepsilon = \frac{1}{2}\left(\mathbf{g} - \mathbf{I}\right) = \begin{pmatrix} \frac{1}{2}(VtY')^2 & 0 \\ 0 & 0 \end{pmatrix} .$$

We can compute the extension resultants $n_{\alpha\beta} = C_{\alpha\beta\gamma\delta}\varepsilon_{\gamma\delta}h_{\text{th}}$ [80, (3.38)] with the given material tensor $C_{\alpha\beta\gamma\delta}$, and obtain

$$\begin{pmatrix} n_{11} \\ n_{22} \\ n_{12} \end{pmatrix} = \frac{Eh_{\text{th}}}{1-\nu^2} \begin{pmatrix} 1 & \nu & 0 \\ \nu & 1 & 0 \\ 0 & 0 & \frac{1-\nu}{2} \end{pmatrix} \begin{pmatrix} \varepsilon_{11} \\ 0 \\ 0 \end{pmatrix} = \frac{Eh_{\text{th}}}{2(1-\nu^2)}(VtY')^2 \begin{pmatrix} 1 \\ \nu \\ 0 \end{pmatrix} , \tag{7.9}$$

where E and ν are the Young's modulus and Poisson's ratio of the membrane material. We now compute the membrane strain variation with respect to the displacement test function $\mathbf{w}$:

$$D_{\mathbf{w}}\varepsilon_{11} = \frac{d}{d\epsilon}\frac{1}{2}\left(\left|\frac{\partial\left(\mathbf{X} + (\mathbf{y} + \epsilon\mathbf{w})\right)}{\partial\xi_1}\right|^2 - 1\right)\Bigg|_{\epsilon=0} = \frac{\partial\left(\mathbf{X} + \mathbf{y}\right)}{\partial\xi_1} \cdot \frac{\partial \mathbf{w}}{\partial\xi_1} \, . \tag{7.10}$$

The internal work term of the variational problem is then

$$\int_{\Gamma_0} \left(\mathbf{n} + \mathbf{n}^{\text{pre}}\right) : D_{\mathbf{w}}\varepsilon \, d\Gamma = \int_{\Gamma_0} n_{11} \frac{\partial\left(\mathbf{X} + \mathbf{y}\right)}{\partial\xi_1} \cdot \frac{\partial \mathbf{w}}{\partial\xi_1} \, d\Gamma \, . \tag{7.11}$$

With the assumption that the test function $\mathbf{w}$ vanishes at the end points of Γ_0, we can integrate by parts to get

$$- \int_{\Gamma_0} \frac{\partial}{\partial\xi_1}\left(\left(n_{11} + n_{11}^{\text{pre}}\right)\frac{\partial}{\partial\xi_1}\left(\mathbf{X} + \mathbf{y}\right)\right) \cdot \mathbf{w} \, d\Gamma \, . \tag{7.12}$$

which yields the strong form of the shell structure subproblem

$$h_{\text{th}}\left(\rho_s\right)_0 \frac{\partial^2 \mathbf{y}}{\partial t^2} - \frac{\partial}{\partial\xi_1}\left(\left(n_{11} + n_{11}^{\text{pre}}\right)\frac{\partial}{\partial\xi_1}\left(\mathbf{X} + \mathbf{y}\right)\right) = -\sqrt{g_{11}}\boldsymbol{\lambda} + h_{\text{th}}\left(\rho_s\right)_0 \mathbf{f}_2 \, , \tag{7.13}$$

where $\sqrt{g_{11}}$ transfers the fluid traction $\boldsymbol{\lambda}$ to the reference configuration. Splitting into components, substituting in the manufactured solution in (7.2), and assuming that the prestress does not vary in space, we get

$$h_{\text{th}}\,(\rho_s)_0\,(\mathbf{f}_2)_1 = -\frac{\partial^2}{\partial\xi_1^2}\left(\frac{3Eh_{\text{th}}}{2(1-\nu^2)}(Vt)^3\left(\frac{\partial Y}{\partial\xi_1}\right)^2 + n_{11}^{\text{pre}}Vt\right)Y + \sqrt{g_{11}}\lambda_1, \tag{7.14}$$

$$h_{\text{th}}\,(\rho_s)_0\,(\mathbf{f}_2)_2 = -\frac{Eh_{\text{th}}}{(1-\nu^2)}(Vt)^2\frac{\partial Y}{\partial\xi_1}\frac{\partial^2 Y}{\partial\xi_1^2} + \sqrt{g_{11}}\lambda_2\,. \tag{7.15}$$

7.4. *Numerical results*

To test the convergence of the projection-based DAL approach to the manufactured solution in the benchmark problem, we take a test problem with the following parameters: $V = 1$, $L = 1$, $P = 1$, $\mu = 0.1$, $\rho_f = 1$, $(\rho_s)_0 = 1$, $n_{11}^{\text{pre}} = 10$, $E = 1$, $h_{\text{th}} = 0.1$, $\nu = 0.3$, and $T = 1$. We then discretize the fluid domain into a uniform grid of $2^N \times 2^N$ lowest-order div-conforming B-spline elements [78, 79], where $N = 4, \ldots, 8$. Weakly-consistent advective stabilization of the form [35, (41)–(43)] is included, but its effect is minimal at such a low Reynolds number. The corresponding time steps are $\Delta t = T/2^N$. The structure is discretized into $19 \times 2^{N-4}$ linear elements along the ξ_1 direction, to ensure some degree of mismatch with the fluid mesh. The FSI penalty parameter β on Γ_t is set to $10\times 2^{N-4}$. The coarse-scale Lagrange multiplier space is discretized in the background fashion proposed in [36]. Dirichlet boundary conditions on $\partial\Omega$ are enforced using a penalty method, with penalty parameter $1000\times 2^{N-4}$. Quadrature on Γ_t is performed using a three-point Gaussian quadrature rule in each element of the membrane structure, without regard to how the structure elements intersect the fluid elements. The nonlinear problem in the implicit step of the semi-implicit algorithm is solved using a fixed number of block iterations [35, Section 4].

A representative numerical solution ($N = 6$) is shown in Figure 11, demonstrating the correct qualitative behavior of the solution. The convergence of the $L^2(\Omega)$ and $H^1(\Omega)$ norms of the velocity errors are shown in the left plot Figure 12; these errors appear to converge at the rates predicted by the analysis of the model problem. The Lagrange multiplier fields as functions of x_2 are shown in the right plot Figure 12; it is evident that there is some $O(1)$ error in $L^2(\Gamma)$, which is again consistent with the analysis of the model problem, in which the multiplier converges in a weak, mesh-dependent norm. The L^∞ deviation from a constant is much less pronounced here than in numerical tests with the model problem.

8. Conclusion

In this paper we present error estimates for the projection-based DAL method (of [36]), for enforcing Dirichlet boundary conditions. We have addressed regularity of immersed Lipschitz interface problems for a simplified linearized parabolic model problem with Lipschitz regular boundary, and provided crucial estimate results for the Dirichlet problem and for the Robin problem. In this model, the computational domain Ω is separated

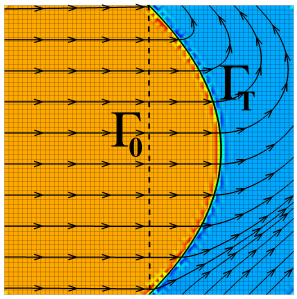

Fig. 11. An annotated snapshot at $t = T$ of a numerical approximation to the manufactured solution. Streamlines indicate fluid velocity. Contours show pressure on a scale from ≤-0.7 (blue) to ≥+0.7 (red), reproducing the expected P of 1, with moderate over- and under-shoot near the structure. (The range of the scale exceeds P to illustrate the over- and under-shoot phenomena.)

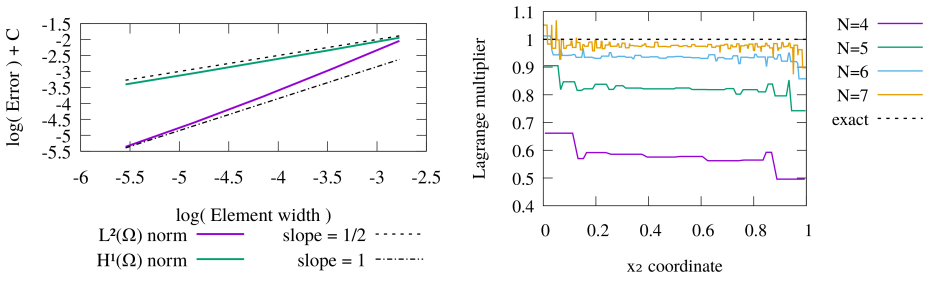

Fig. 12. Computational results in the FSI benchmark problem, from projection-based DAL method. Left: Convergence of the fluid velocity error at time T in the $H^1(\Omega)$ and $L^2(\Omega)$ norms. Right: The Lagrange multiplier at time T, for various meshes, interpolated linearly between samples at quadrature points on Γ_T.

by a co-dimension one interface Γ which is Lipschitz regular, and a Dirichlet boundary condition is enforced on Γ. We have shown that for both 2D and 3D cases, when both the initial condition and the loadings present sufficient smoothness ($u_0 \in C^4(\Omega)$, $f_i \in C^2(\Omega_i \times (0,T))$, $g \in C^3(0,T;H^1_0(\Gamma))$) the solution $u(\mathbf{x},t)$ for this problem has regularity $u \in H^2(0,T;H^{3/2-\epsilon}(\Omega))$ and the normal jump of its gradient $\lambda \in H^1(0,T;L^2(\Gamma))$, for any $\epsilon > 0$. With this regularity, we have for the first time provided sharp error estimates for the projection-based DAL method: When the element size on Ω is h, and the element size for the Lagrange multiplier is H, large enough, with penalty parameter $\beta = O(1/h)$, the following error estimates hold for $0 < \epsilon \ll \frac{1}{2}$:

$$\left|\left|\left|(u(t^{n+1}) - u_h^{n+1}, \lambda(t^{n+1}) - \lambda_H^{n+1})\right|\right|\right|_p^2 \leq C\left(\frac{h^{1-2\epsilon}H}{\Delta t} + \Delta t\right)\left(\int_0^{t^{n+1}} \left\|\frac{\partial u}{\partial t}\right\|^2_{H^{3/2-\epsilon}(\Omega)} + \left\|\frac{\partial \lambda}{\partial t}\right\|^2_{L^2(\Gamma)} + \left\|\frac{\partial^2 u}{\partial t^2}\right\|^2_{L^2(\Omega)} dt + \|u_0\|^2_{H^{3/2-\epsilon}(\Omega)} + \|\lambda_0\|^2_{L^2(\Gamma)}\right),$$

$$\left\|u(t^{n+1}) - u_h^{n+1}\right\|^2_{L^2(\Omega)} \leq C(h^{1-2\epsilon}H + \Delta t^2)\left(\int_0^{t^{n+1}} \left\|\frac{\partial u}{\partial t}\right\|^2_{H^{3/2-\epsilon}(\Omega)} + \left\|\frac{\partial \lambda}{\partial t}\right\|^2_{L^2(\Gamma)} + \left\|\frac{\partial^2 u}{\partial t^2}\right\|^2_{L^2(\Omega)} dt + \|u_0\|^2_{H^{3/2-\epsilon}(\Omega)} + \|\lambda_0\|^2_{L^2(\Gamma)}\right).$$

The results suggest the optimal choice of time-step size as $\Delta t = O(h) = O(H)$, which yields approximately half-order accuracy for u in the $H^1(\Omega)$ norm, and first-order accuracy of u in the $L^2(\Omega)$ norm. Given the problem regularity, the convergence rate in $H^1(\Omega)$ is the same as the rates from the Lagrange-multiplier based fictitious-domain method [22, 53], which is actually the best possible rate when using a quasi-uniform mesh of Ω that is not designed to conform to the boundary Γ.

In the numerical investigations, we have firstly verified the error estimates on numerical tests using the model problem. To test the applicability of the above error estimates in practice for more complicated applications, i.e., in the immersogemetric methods for nonlinear and large-displacement FSI, we have derived a novel manufactured solution for a fluid-thin structure problem with pressure jump. Numerical evidence has suggested that on this FSI benchmark problem, the approximate fluid velocity converges at the predicted rates to the manufactured solution.

Acknowledgements

Y. Yu would like to acknowledge the support from National Science Foundation under Award No. DMS-1620434 and the Simons collaboration grant 360504. D. Kamensky and Y. Bazilevs were supported through AFOSR Award No. FA9550-16-1-0131. M.-C. Hsu and T.J.R. Hughes were supported by NIH/NHLBI Award No. R01HL129077. T.J.R. Hughes was also supported by ONR grants No. N00014-17-1-2119 and No. N00014-13-1-0500. X.Y. Lu was partially supported by Lakehead University funding no. 10-50-16422410 and 10-50-16422409, and by NSERC Discovery Grant no. 10-50-16420120. Part of this work was performed when X.Y. Lu was a postdoc at McGill University. The authors also want to express their appreciation of the critical reviews made by an anonymous reviewer, which improved the clarity and quality of this work.

References

1. Y. Bazilevs, K. Takizawa, and T. E. Tezduyar. *Computational Fluid–Structure Interaction: Methods and Applications*. Wiley, Chichester, 2013.
2. C. S. Peskin. Flow patterns around heart valves: A numerical method. *Journal of Computational Physics*, 10(2):252–271, 1972.
3. Boyce E Griffith. Immersed boundary model of aortic heart valve dynamics with physiological driving and loading conditions. *International Journal for Numerical Methods in Biomedical Engineering*, 28(3):317–345, 2012.
4. F. Nobile. Coupling strategies for the numerical simulation of blood flow in deformable arteries by 3D and 1D models. *Mathematical and Computer Modelling*, 49(11-12):2152–2160, 2009.

5. F. Nobile and C. Vergara. An effective fluid-structure interaction formulation for vascular dynamics by generalized Robin conditions. *SIAM Journal on Scientific Computing*, 30(2):731–763, 2008.
6. M. Astorino, F. Chouly, and M. A. Fernández. Robin based semi-implicit coupling in fluid-structure interaction: Stability analysis and numerics. *SIAM Journal on Scientific Computing*, 31(6):4041–4065, 2009.
7. S. Badia, F. Nobile, and C. Vergara. Fluid-structure partitioned procedures based on Robin transmission conditions. *Journal of Computational Physics*, 227(14):7027–7051, 2008.
8. Santiago. Badia, F. Nobile, and C. Vergara. Robin-Robin preconditioned Krylov methods for fluid-structure interaction problems. *Computer Methods in Applied Mechanics and Engineering*, 198(33-36):2768–2784, 2009.
9. M. W. Gee, U. Kuttler, and W. A. Wall. Truly monolithic algebraic multigrid for fluid-structure interaction. *International Journal for Numerical Methods in Engineering*, 85(8):987–1016, 2011.
10. J. Degroote and J. Vierendeels. Multi-solver algorithms for the partitioned simulation of fluid-structure interaction. *Computer Methods in Applied Mechanics and Engineering*, 200(25-28):2195–2210, 2011.
11. M. M. Joosten, W. G. Dettmer, and D. Peric. Analysis of the block Gauss-Seidel solution procedure for a strongly coupled model problem with reference to fluid-structure interaction. *International Journal for Numerical Methods in Engineering*, 78(7):757–778, 2009.
12. G. Guidoboni, R. Glowinski, N. Cavallini, and S. Canic. Stable loosely-coupled-type algorithm for fluid-structure interaction in blood flow. *Journal of Computational Physics*, 228(18):6916–6937, 2009.
13. C. Michler, H. van Brummelen, and R. de Borst. An investigation of interface-GMRES(R) for fluid-structure interaction problems with flutter and divergence. *Computational Mechanics*, 47(1):17–29, 2011.
14. F. X. Roux and J. D. Garaud. Domain decomposition methodology with Robin interface matching conditions for solving strongly coupled fluid-structure problems. *International Journal for Multiscale Computational Engineering*, 7(1):29–38, 2009.
15. H. Baek and G. E. Karniadakis. A convergence study of a new partitioned fluid-structure interaction algorithm based on fictitious mass and damping. *Journal of Computational Physics*, 231(2):629–652, 2012.
16. C. S. Peskin. The immersed boundary method. *Acta Numerica*, 11:479–517, 2002.
17. R. Mittal and G. Iaccarino. Immersed boundary methods. *Annual Review of Fluid Mechanics*, 37:239–261, 2005.
18. F. Sotiropoulos and X. Yang. Immersed boundary methods for simulating fluid–structure interaction. *Progress in Aerospace Sciences*, 65:1–21, 2014.
19. K. Takizawa and T. E. Tezduyar. Computational methods for parachute fluid–structure interactions. *Archives of Computational Methods in Engineering*, 19:125–169, 2012.
20. Y. Bazilevs, J. R. Gohean, T. J. R. Hughes, R. D. Moser, and Y. Zhang. Patient-specific isogeometric fluid–structure interaction analysis of thoracic aortic blood flow due to

implantation of the Jarvik 2000 left ventricular assist device. *Computer Methods in Applied Mechanics and Engineering*, 198:3534–3550, 2009.
21. M.-C. Hsu and Y. Bazilevs. Fluid–structure interaction modeling of wind turbines: simulating the full machine. *Computational Mechanics*, 50:821–833, 2012.
22. D. Boffi and L. Gastaldi. A fictitious domain approach with Lagrange multiplier for fluid-structure interactions. *Numerische Mathematik*, 135(3):711–732, 2017.
23. Fredrik Bengzon and Mats G Larson. Adaptive finite element approximation of multiphysics problems: A fluid–structure interaction model problem. *International Journal for Numerical Methods in Engineering*, 84(12):1451–1465, 2010.
24. E. Burman and M. A. Fernández. Stabilization of explicit coupling in fluid-structure interaction involving fluid incompressibility. *Computer Methods in Applied Mechanics and Engineering*, 198(5-8):766–784, 2009.
25. M Bukač, Ivan Yotov, Rana Zakerzadeh, and Paolo Zunino. Partitioning strategies for the interaction of a fluid with a poroelastic material based on a nitsches coupling approach. *Computer Methods in Applied Mechanics and Engineering*, 292:138–170, 2015.
26. Alexander Lozovskiy, Maxim A Olshanskii, Victoria Salamatova, and Yuri V Vassilevski. An unconditionally stable semi-implicit fsi finite element method. *Computer Methods in Applied Mechanics and Engineering*, 297:437–454, 2015.
27. C. Wang, M. C. H. Wu, F. Xu, M.-C. Hsu, and Y. Bazilevs. Modeling of a hydraulic arresting gear using fluid–structure interaction and isogeometric analysis. *Computers & Fluids*, 142:3–14, 2017.
28. M. C. H. Wu, D. Kamensky, C. Wang, A. J. Herrema, F. Xu, M. S. Pigazzini, A. Verma, A. L. Marsden, Y. Bazilevs, and M.-C. Hsu. Optimizing fluid–structure interaction systems with immersogeometric analysis and surrogate modeling: Application to a hydraulic arresting gear. *Computer Methods in Applied Mechanics and Engineering*, 316:668–693, 2017.
29. A. Quarteroni and L. Formaggia. Mathematical modelling and numerical simulation of the cardiovascular system. In N. Ayache, editor, *Computational Models for the Human Body*, volume 12 of *Handbook of Numerical Analysis*, pages 3 – 127. Elsevier, 2004.
30. Yue Yu, Fangfang Xie, Hongmei Yan, Yiannis Constantinides, Owen Oakley, and George Em Karniadakis. Suppression of vortex-induced vibrations by fairings: A numerical study. *Journal of Fluids and Structures*, 54:679–700, 2015.
31. D. Kamensky, M.-C. Hsu, D. Schillinger, J. A. Evans, A. Aggarwal, Y. Bazilevs, M. S. Sacks, and T. J. R. Hughes. An immersogeometric variational framework for fluid–structure interaction: Application to bioprosthetic heart valves. *Computer Methods in Applied Mechanics and Engineering*, 284:1005–1053, 2015.
32. M.-C. Hsu, D. Kamensky, Y. Bazilevs, M. S. Sacks, and T. J. R. Hughes. Fluid–structure interaction analysis of bioprosthetic heart valves: significance of arterial wall deformation. *Computational Mechanics*, 54:1055–1071, 2014.
33. M.-C. Hsu, D. Kamensky, F. Xu, J. Kiendl, C. Wang, M. C. H. Wu, J. Mineroff, A. Reali, Y. Bazilevs, and M. S. Sacks. Dynamic and fluid–structure interaction simulations of bioprosthetic heart valves using parametric design with T-splines and Fung-type

material models. *Computational Mechanics*, 55:1211–1225, 2015.

34. D. Kamensky, J. A. Evans, and M.-C. Hsu. Stability and conservation properties of collocated constraints in immersogeometric fluid-thin structure interaction analysis. *Communications in Computational Physics*, 18:1147–1180, 2015.
35. D. Kamensky, M.-C. Hsu, Y. Yu, J. A. Evans, M. S. Sacks, and T. J. R. Hughes. Immersogeometric cardiovascular fluid–structure interaction analysis with divergence-conforming B-splines. *Computer Methods in Applied Mechanics and Engineering*, 314:408–472, 2017.
36. D. Kamensky, J. A. Evans, M.-C. Hsu, and Y. Bazilevs. Projection-based stabilization of interface Lagrange multipliers in immersogeometric fluid–thin structure interaction analysis, with application to heart valve modeling. *Computers and Mathematics with Applications*, 74(9):2068–2088, 2017.
37. P. Hansbo and J. Hermansson. Nitsche's method for coupling non-matching meshes in fluid-structure vibrational problems. *Computational Mechanics*, 32:134–139, 2003.
38. André Massing, Mats Larson, Anders Logg, and Marie Rognes. A nitsche-based cut finite element method for a fluid-structure interaction problem. *Communications in Applied Mathematics and Computational Science*, 10(2):97–120, 2015.
39. Erik Burman, Peter Hansbo, Mats G Larson, and Sara Zahedi. Cut finite element methods for coupled bulk–surface problems. *Numerische Mathematik*, 133(2):203–231, 2016.
40. J. S. Soares, K. R. Feaver, W. Zhang, D. Kamensky, A. Aggarwal, and M. S. Sacks. Biomechanical behavior of bioprosthetic heart valve heterograft tissues: Characterization, simulation, and performance. *Cardiovascular Engineering and Technology*, 7(4):309–351, 2016.
41. Joao S Soares, Kristen R Feaver, Will Zhang, David Kamensky, Ankush Aggarwal, and Michael S Sacks. Biomechanical behavior of bioprosthetic heart valve heterograft tissues: Characterization, simulation, and performance. *Cardiovascular engineering and technology*, 7(4):309–351, 2016.
42. Gil Marom. Numerical methods for fluid–structure interaction models of aortic valves. *Archives of Computational Methods in Engineering*, 22(4):595–620, 2015.
43. Arash Kheradvar, Elliott M Groves, Ahmad Falahatpisheh, Mohammad K Mofrad, S Hamed Alavi, Robert Tranquillo, Lakshmi P Dasi, Craig A Simmons, K Jane Grande-Allen, Craig J Goergen, et al. Emerging trends in heart valve engineering: part iv. computational modeling and experimental studies. *Annals of biomedical engineering*, 43(10):2314–2333, 2015.
44. J. Kiendl, K.-U. Bletzinger, J. Linhard, and R. Wüchner. Isogeometric shell analysis with Kirchhoff–Love elements. *Computer Methods in Applied Mechanics and Engineering*, 198:3902–3914, 2009.
45. E. H. van Brummelen. Added mass effects of compressible and incompressible flows in fluid–structure interaction. *Journal of Applied Mechanics*, 76:021206, 2009.
46. Erik Burman, Johnny Guzmán, Manuel A Sánchez, and Marcus Sarkis. Robust flux error estimation of nitsches method for high contrast interface problems. *arXiv preprint arXiv:1602.00603*, 2016.

47. T. J. R. Hughes, J. A. Cottrell, and Y. Bazilevs. Isogeometric analysis: CAD, finite elements, NURBS, exact geometry and mesh refinement. *Computer Methods in Applied Mechanics and Engineering*, 194:4135–4195, 2005.
48. J. A. Cottrell, T. J. R. Hughes, and Y. Bazilevs. *Isogeometric Analysis: Toward Integration of CAD and FEA*. Wiley, Chichester, 2009.
49. F. Xu, D. Schillinger, D. Kamensky, V. Varduhn, C. Wang, and M.-C. Hsu. The tetrahedral finite cell method for fluids: Immersogeometric analysis of turbulent flow around complex geometries. *Computers & Fluids*, 141:135–154, 2016.
50. M.-C. Hsu, C. Wang, F. Xu, A. J. Herrema, and A. Krishnamurthy. Direct immersogeometric fluid flow analysis using B-rep CAD models. *Computer Aided Geometric Design*, 43:143–158, 2016.
51. C. Wang, F. Xu, M.-C. Hsu, and A. Krishnamurthy. Rapid B-rep model preprocessing for immersogeometric analysis using analytic surfaces. *Computer Aided Geometric Design*, 52–53:190–204, 2017.
52. R. Glowinski, T.-W. Pan, and J. Periaux. A fictitious domain method for Dirichlet problem and applications. *Computer Methods in Applied Mechanics and Engineering*, 111(3):283–303, 1994.
53. R. Glowinski, T.-W. Pan, T. I. Hesla, and D. D. Joseph. A distributed Lagrange multiplier/fictitious domain method for particulate flows. *International Journal of Multiphase Flow*, 25(5):755–794, 1999.
54. D. Boffi, N. Cavallini, and L. Gastaldi. The finite element immersed boundary method with distributed Lagrange multiplier. *SIAM Journal on Numerical Analysis*, 53(6):2584–2604, 2015.
55. M. R. Hestenes. Multiplier and gradient methods. *Journal of Optimization Theory and Applications*, 4(5):303–320, 1969.
56. M. J. D. Powell. A method for nonlinear constraints in minimization problems. In R. Fletcher, editor, *Optimization*, pages 283–298. Academic Press, New York, 1969.
57. J. C. Simo and T. A. Laursen. An augmented Lagrangian treatment of contact problems involving friction. *Computers & Structures*, 42(1):97–116, 1992.
58. D. Goldstein, R. Handler, and L. Sirovich. Modeling a no-slip flow boundary with an external force field. *Journal of Computational Physics*, 105(2):354–366, 1993.
59. D. B. Goldstein and T.-C. Tuan. Secondary flow induced by riblets. *Journal of Fluid Mechanics*, 363:115–151, 1998.
60. J. S. Strand and D. B. Goldstein. Application of passive surface textures to control the growth of turbulent spots at moderately high reynolds numbers. *International Journal of Flow Control*, 2:73–89, 2010.
61. J. S. Strand and D. B. Goldstein. Direct numerical simulations of riblets to constrain the growth of turbulent spots. *Journal of Fluid Mechanics*, 668:267–292, 2011.
62. C. J. Doolittle, S. D. Drews, and D. B. Goldstein. Near-field flow structures about subcritical surface roughness. *Physics of Fluids*, 26:124106, 2014.
63. D. J. Benson and S. Okazawa. Contact in a multi-material Eulerian finite element formulation. *Computer Methods in Applied Mechanics and Engineering*, 193(39):4277–4298, 2004.

64. A. Haufe, K. Weimar, and U. Göhner. Advanced airbag simulation using fluid-structure-interaction and the Eluerian method in LS-DYNA. In *Proceedings of the LS-DYNA Anwenderforum*, 2004.
65. G. G. Chew, I. C. Howard, and E. A. Patterson. Simulation of damage in a porcine prosthetic heart valve. *Journal of Medical Engineering & Technology*, 23(5):178–189, 1999.
66. C. J. Carmody, G. Burriesci, I. C. Howard, and E. A. Patterson. An approach to the simulation of fluid–structure interaction in the aortic valve. *Journal of Biomechanics*, 39:158–169, 2006.
67. F. Sturla, E. Votta, M. Stevanella, C. A. Conti, and A. Redaelli. Impact of modeling fluid–structure interaction in the computational analysis of aortic root biomechanics. *Medical Engineering and Physics*, 35:1721–1730, 2013.
68. W. Wu, D. Pott, B. Mazza, T. Sironi, E. Dordoni, C. Chiastra, L. Petrini, G. Pennati, G. Dubini, U. Steinseifer, S. Sonntag, M. Kuetting, and F. Migliavacca. Fluid–structure interaction model of a percutaneous aortic valve: Comparison with an in vitro test and feasibility study in a patient-specific case. *Annals of Biomedical Engineering*, 44(2):590–603, 2016.
69. M. Souli, Y. Sofiane, and L. Olovsson. ALE and fluid/structure interaction in LS-DYNA. In *Proceedings of Emerging Technology in Fluids, Structures, and Fluid–Structure Interactions*. ASME, 2004.
70. M. Souli, N. Capron, and U. Khan. Fluid structure interaction and airbag ALE for out of position. In *Proceedings of the ASME Pressure Vessels and Piping Conference*. AMSE, 2005.
71. M. Souli, J. Wang, I. Do, and C. Hao. ALE and fluid structure interaction in LS-DYNA. In *Proceedings of the 8th International LS-DYNA Users Conference*, 2011.
72. Marius Mitrea. The initial Dirichlet boundary value problem for general second order parabolic systems in nonsmooth manifolds. *Communications in Partial Differential Equations*, 26(11-12):1975–2036, 2001.
73. Y. Bazilevs, M.-C. Hsu, and M. A. Scott. Isogeometric fluid–structure interaction analysis with emphasis on non-matching discretizations, and with application to wind turbines. *Computer Methods in Applied Mechanics and Engineering*, 249–252:28–41, 2012.
74. M. Esmaily-Moghadam, Y. Bazilevs, T.-Y. Hsia, I. E. Vignon-Clementel, A. L. Marsden, and Modeling of Congenital Hearts Alliance (MOCHA). A comparison of outlet boundary treatments for prevention of backflow divergence with relevance to blood flow simulations. *Computational Mechanics*, 48:277–291, 2011.
75. J. A. Evans. *Divergence-free B-spline Discretizations for Viscous Incompressible Flows*. Ph.D. thesis, University of Texas at Austin, Austin, Texas, United States, 2011.
76. J. A. Evans and T. J. R. Hughes. Isogeometric divergence-conforming B-splines for the steady Navier–Stokes equations. *Mathematical Models and Methods in Applied Sciences*, 23(08):1421–1478, 2013.
77. J. A. Evans and T. J. R. Hughes. Isogeometric divergence-conforming B-splines for the unsteady Navier–Stokes equations. *Journal of Computational Physics*, 241:141–167,

2013.

78. A. Buffa, G. Sangalli, and R. Vázquez. Isogeometric analysis in electromagnetics: B-splines approximation. *Computer Methods in Applied Mechanics and Engineering*, 199(17–20):1143–1152, 2010.
79. A. Buffa, J. Rivas, G. Sangalli, and R. Vásquez. Isogeometric discrete differential forms in three dimensions. *SIAM Journal on Numerical Analysis*, 49(2):814–844, 2011.
80. J. Kiendl. *Isogeometric Analysis and Shape Optimal Design of Shell Structures*. PhD thesis, Lehrstuhl für Statik, Technische Universität München, 2011.
81. J. Kiendl, M.-C. Hsu, M. C. H. Wu, and A. Reali. Isogeometric Kirchhoff–Love shell formulations for general hyperelastic materials. *Computer Methods in Applied Mechanics and Engineering*, 291:280–303, 2015.
82. Y. Bazilevs and T. J. R. Hughes. Weak imposition of Dirichlet boundary conditions in fluid mechanics. *Computers and Fluids*, 36:12–26, 2007.
83. Y. Bazilevs, C. Michler, V. M. Calo, and T. J. R. Hughes. Weak Dirichlet boundary conditions for wall-bounded turbulent flows. *Computer Methods in Applied Mechanics and Engineering*, 196:4853–4862, 2007.
84. Y. Bazilevs, C. Michler, V. M. Calo, and T. J. R. Hughes. Isogeometric variational multiscale modeling of wall-bounded turbulent flows with weakly enforced boundary conditions on unstretched meshes. *Computer Methods in Applied Mechanics and Engineering*, 199:780–790, 2010.
85. M.-C. Hsu, I. Akkerman, and Y. Bazilevs. Wind turbine aerodynamics using ALE–VMS: Validation and the role of weakly enforced boundary conditions. *Computational Mechanics*, 50:499–511, 2012.
86. P. M. Pinsky. A finite element formulation for elastoplasticity based on a three-field variational equation. *Computer Methods in Applied Mechanics and Engineering*, 61(1):41–60, 1987.
87. C. Hager and B. I. Wohlmuth. Nonlinear complementarity functions for plasticity problems with frictional contact. *Computer Methods in Applied Mechanics and Engineering*, 198(41):3411–3427, 2009.
88. J. Chung and G. M. Hulbert. A time integration algorithm for structural dynamics with improved numerical dissipation: The generalized-α method. *Journal of Applied Mechanics*, 60:371–75, 1993.
89. Y. Bazilevs, V. M. Calo, T. J. R. Hughes, and Y. Zhang. Isogeometric fluid–structure interaction: theory, algorithms, and computations. *Computational Mechanics*, 43:3–37, 2008.
90. J.L. Lions and E. Magenes. *Non-homogeneous boundary value problems and applications*. Number v. 1 in Non-homogeneous Boundary Value Problems and Applications. Springer-Verlag, 1972.
91. Ivo Babuška. The finite element method with Lagrangian multipliers. *Numerische Mathematik*, 20(3):179–192, 1973.
92. Ajit Patel. Lagrange multiplier method with penalty for elliptic and parabolic interface problems. *Journal of Applied Mathematics and Computing*, 37(1-2):37–56, 2011.

93. David Jerison and Carlos E Kenig. The inhomogeneous Dirichlet problem in Lipschitz domains. *Journal of functional analysis*, 130(1):161–219, 1995.
94. S. E. Mikhailov. Traces, extensions, co-normal derivatives and solution regularity of elliptic systems with smooth and non-smooth coefficients. *available at* `http://www.sciencedirect.com/science/article/pii/S0022247X10010358`.
95. Martin Costabel, Monique Dauge, and Serge Nicaise. Analytic regularity for linear elliptic systems in polygons and polyhedra. *Mathematical Models and Methods in Applied Sciences*, 22(08):1250015, 2012.
96. M.-C. Lai and C. S. Peskin. An immersed boundary method with formal second-order accuracy and reduced numerical viscosity. *Journal of Computational Physics*, 160(2):705–719, 2000.
97. L. C. Evans. *Partial Differential Equations (Graduate Studies in Mathematics, Vol. 19)*. American Mathematical Society, Providence, Rhode Island, 2002.
98. M. A. Puso, J. Sanders, R. Settgast, and B. Liu. An embedded mesh method in a multiple material ALE. *Computer Methods in Applied Mechanics and Engineering*, 245–246:273–289, 2012.
99. M.-C. Hsu and Y. Bazilevs. Blood vessel tissue prestress modeling for vascular fluid–structure interaction simulations. *Finite Elements in Analysis and Design*, 47:593–599, 2011.